Design and Additive Manufacturing of a Transfemoral Prosthetic Socket

CN Genis

orcid.org/ 0000-0002-3689-4187

Dissertation accepted in fulfilment of the requirements for the degree *Master of Engineering in Mechanical Engineering* at the North-West University

Supervisor: Dr A Bayode

Co-supervisor: Mr L Nyanga

Graduation: May 2026

ACKNOWLEDGEMENTS

- Our Heavenly Father for His grace and blessings of strength, knowledge and resilience.
- My incredible wife, Nolene, for all her love and support throughout my studies.
- My parents, Ben and Charlotte, for their love, effort, emotional and financial support
- My supervisors, Dr. Bayode and Mr. Nyanga, for their guidance, support and patience.
- JP van Deventer and Ian Thompson for their assistance with manufacturing and other practical aspects of the study.

ABSTRACT

Traditional manufacturing of transfemoral (TF) prosthetic sockets relies on labour-intensive casting and lamination processes that are costly, time-consuming, and difficult to standardise. As additive manufacturing (AM) technologies—particularly fused deposition modelling (FDM)—continue to advance in affordability and reliability, they present an opportunity to streamline prosthetic production while enabling greater repeatability, digital control, and accessibility. This study addresses the need for a more efficient and cost-effective alternative by designing and manufacturing a TF prosthetic socket specifically for AM and evaluating its structural performance against regulatory loading requirements.

A patient-specific socket geometry was obtained by 3D scanning an existing TF socket and processing the resulting mesh in MeshMixer before generating two design variants in SOLIDWORKS. Each design underwent linear static finite element analysis (FEA) to identify critical stress regions and compare relative structural performance under ISO 10328 loading condition P5. Based on these simulations, a final design was selected for fabrication. Sockets were manufactured using FDM with polyethylene terephthalate glycol (PETG) filament, chosen for its favourable printability and availability. The final PETG sockets were subjected to ultimate static strength testing in accordance with ISO 10328 P5 [I] using a uniaxial testing machine. Only PETG specimens were tested.

The PETG sockets successfully exceeded the ultimate test force of the P5 [I] loading condition. One specimen was loaded to failure, which occurred at 7.2 kN through a brittle fracture at the distal end. The fracture propagated along and across layer lines, indicating strong interlayer adhesion. Additional sockets were loaded to 5 kN—beyond the ISO 10328 requirement—to avoid equipment damage, and no visible deformation or structural compromise was observed. The failure location and fracture propagation pattern corresponded qualitatively with the high-stress regions predicted by FEA, demonstrating that the simulations were effective as a comparative design tool.

Overall, the findings demonstrate that PETG is a suitable material for FDM-manufactured TF prosthetic sockets and is capable of meeting the ultimate static strength requirement specified by ISO 10328 P5 [I]. While the results confirm the viability of PETG sockets under static loading, further testing—including cyclic loading and additional ISO 10328 requirements—is necessary to establish full regulatory compliance. Nevertheless, the successful performance of PETG, combined with its printability and widespread availability, highlights its potential for producing accessible, low-cost, and digitally manufactured TF prosthetic sockets.

Keywords: Additive Manufacturing, Design, Fused Deposition Modelling (FDM), ISO 10328, Transfemoral Prosthetic Socket.

LIST OF ABBREVIATIONS

AKA	Above-Knee Amputation/Amputee
AM	Additive Manufacturing
CAD	Computer Aided Design
CF	Carbon Fibre
ePA-CF	Engineering Polyamide Carbon Fibre
FDM	Fused Deposition Modelling
PETG	Polyethylene terephthalate glycol
SLA	Stereolithography
TF	Transfemoral
TT	Transtibial

TABLE OF CONTENTS

LIST OF TABLES

LIST OF FIGURES

CHAPTER 1: INTRODUCTION

1.1 Background

The design and development of transfemoral (TF) prosthetic sockets have long been critical components in the field of prosthetics, aiming to improve the quality of life of individuals with above-knee amputations (AKA). AKA is the process of removing a patient's leg by cutting through the femoral bone and thigh tissue at a case-specific distance above the knee. A variety of medical reasons, such as trauma, infection, tumour, or vascular compromise, can lead to this procedure (Myers & Chauvin, 2021). Following AKA, patients require TF prostheses to be able to walk again and consequently improve their quality of life. Acquiring suitable prostheses is usually a costly process, which limits the opportunity for all amputees to regain some functionality and quality of life.

Traditional manufacturing of TF prosthetic sockets typically involves test sockets, which are generally made of plastic, while definitive sockets are laminated and can be made of carbon fibre, fibreglass, or nylon materials (Engstrom & Van de Ven, 1999). These manufacturing methods are time-consuming and expensive (Pousett et al., 2019). Between 6 and 16 weeks pass from amputation to delivery of lower limb prostheses in high-income countries (Johannesson et al., 2010; Kamrad et al., 2020). The manual labour required for the moulding, fitting and adjustments of these sockets requires the expertise of a qualified prosthetist, adding significant time and cost to the process. The typical laminated interface procedure, which involves casting, checking sockets, and laminated definitive interface, has been reported to take at least 14 days to fabricate (Marable et al., 2020). Reducing the time spent in rehabilitation can also reduce prosthesis costs by up to 25% (Miller et al., 2020). Finally, several fittings and rectifications by a skilled prosthetist are required before the final handover to the customer. As a result, many amputees face financial and logistical barriers when acquiring well-fitted prosthetic devices, limiting their ability to regain function and improve their overall quality of life.

Almost 40 years ago, Krouskop et al. (1987) already predicted that computer-aided design (CAD) technology can be used to reduce manufacturing time and cost. 3D scanning allows for the precise capture of the residual limb's geometry, enabling the creation of highly accurate digital models. These models can then be imported into the CAD software, where they can be customised and optimised for a perfect fit. The ability to digitally store and modify these designs enhances the flexibility and repeatability of the manufacturing process. The integration of digital tools like 3D scanning and CAD enhances design accuracy and efficiency.

Recent advances in digital technologies and additive manufacturing (AM) offer a transformative opportunity in specific fields to further reduce manufacturing time and costs. AM offers certain advantages over traditional subtractive manufacturing methods like reduced material waste and allowing greater design flexibility. Since its inception in the 1980s, the use of AM has increased significantly, especially in the past decade, enabling the production of highly customised and complex parts without the need for specialised tooling (Wong & Hernandez, 2012). Fused Deposition Modelling (FDM) is the AM method most commonly used in prosthetic socket research due to its affordability and accessibility; the process involves layer-by-layer extrusion of molten thermoplastic to build the final part (Oldfrey et al., 2020). Chen et al. (2016) investigated the method for integrating 3D scanning, computer-aided design (CAD), and 3D printing. It was found evident that AM has advanced and is beneficial for creating personalised orthoses and prostheses, improving on traditional manufacturing methods which involve laborious steps and lengthy fabrication times. Studies have shown that 3D printing can cut manufacturing times by up to 75% compared to conventional methods, with some cases achieving same-day prosthetic delivery (Borthakur, 2025). In addition to shorter manufacturing times AM also results in reduced production costs for prosthetic devices due to lower raw material costs (Al-Masa'fah et al., 2025)

The use of finite element analysis (FEA) simulation software further enhances the design process by allowing for virtual stress testing, design selection and optimisation of the socket's structure before physical manufacturing and testing. FEA is widely used in biomechanics as a useful tool for predicting stress and strain for a better understanding of load transfer in prostheses (Jia et al., 2004). To ensure that the final product meets the necessary strength and durability requirements, physical testing in accordance with an industry standard such as ISO 10328 is required. This standard specifies procedures for testing the static and cyclic strength of lower limb prostheses, ensuring that the designed prosthetic sockets can withstand the mechanical loads experienced during extreme cases and typical use (ISO10328, 2016). For this study only static loading will be considered.

By adopting these advanced technologies, the production of TF prosthetic sockets can be significantly streamlined. The combination of digital precision and AM can not only reduce the time and cost associated with traditional fabrication methods but also has the potential to improve the overall quality and customisation of prosthetics. This approach also has the potential to make high-quality prosthetic care more accessible to a larger population of amputees, ultimately improving their mobility and quality of life.

1.2 Problem Statement

The traditional manufacturing process for TF prosthetic sockets is often costly and time-consuming, indicating a need for improvement. The growing affordability of AM, particularly FDM, presents an opportunity to enhance the socket manufacturing process. Therefore, it is essential to design, manufacture, and test a TF prosthetic socket using FDM to evaluate the feasibility (according to ISO 10328) of this more cost-effective and time-efficient alternative.

1.3 Research Aim

The study aims to design and manufacture a custom TF socket using FDM and test it to ensure compliance with regulatory standards.

1.4 Objectives

The objectives of this study were the following:

- Determine whether a TF prosthetic socket designed through 3D scanning and CAD modelling, can produce a geometrically accurate and clinically viable socket geometry.
- Assess how design variations of TF socket geometry influence stress distribution and critical failure conditions under ISO 10328 P5 loading using FEA.
- Evaluate the ultimate static strength and failure mode of FDM-manufactured TF sockets under ISO 10328 P5 loading conditions.
- Assess the correlation between FEA-predicted high-stress regions and experimentally observed fracture locations in the TF sockets.

1.5 Design Assumptions and Considerations

- The geometry obtained from the 3D scan of the TF check socket was assumed to accurately represent a well-fitting socket for the amputee from whom it was derived.
- It was assumed that the alignment prescribed by the prosthetist in the original check socket provided an appropriate reference for the design orientation.
- The materials in this study were assumed to behave as isotropic and homogeneous in the FEA, even though FDM-manufactured parts are naturally anisotropic.

- Material properties were based on available manufacturer data and literature values, assumed representative of the actual printed materials for the purpose of a comparative analysis.
- Boundary conditions of the FEA setup were assumed to replicate the ISO 10328:2016 test configuration sufficiently.

1.6 Dissertation Outline

The dissertation is structured into five chapters. Chapter 1 introduces the study by detailing the background and context of the research, defining the problem statement, research aim, objectives, scope, and fundamental assumptions of the study. Chapter 2 offers a comprehensive overview of relevant literature, focusing on prosthetic socket design and manufacturing, AM methods, FEA, and the implementation of ISO 10328 for structural evaluation. Chapter 3 reports the methodology followed in this study, covering the procedures of 3D scanning, CAD modelling, and material selection, along with the FEA simulations performed to inform design selection prior to physical testing. Chapter 4 presents and analyses the experimental testing outcomes, assessing the structural performance and failure behaviour of the additively manufactured sockets under ISO 10328 loading conditions. Chapter 5 finally summarises the key findings of the research, draws the main conclusions, and offers recommendations for subsequent studies and the further development of additively manufactured prosthetic sockets.

CHAPTER 2: LITERATURE REVIEW

2.1 Introduction

This provides a more in-depth background on the design and manufacturing of prosthetic sockets, as well as the technology used in the study. The technology discussed includes AM, focusing on FDM and materials, 3D scanning and ISO 10328 as a testing standard.

2.2 Prosthetic Socket Design

Prosthetic sockets for AKA's form part of a complex lower limb prosthesis, consisting of the socket, knee system, shank/pylon, ankle, and foot, as illustrated in Figure 2.1. With each component playing a critical role in the functionality and comfort of the prosthesis, the prosthetic socket is the primary and critical interface between the amputee's residual limb and the rest of the prosthesis. As the human-machine interface, the prosthetic socket remains the greatest challenge in the world of prostheses.

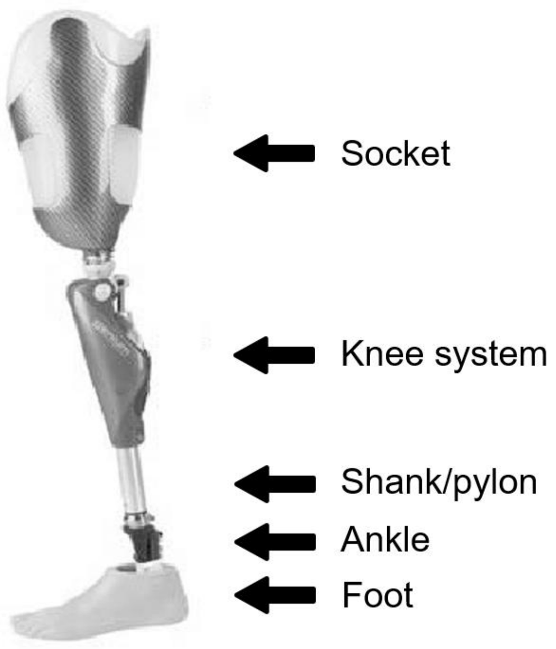

Figure 2.1: Components of Advanced Lower Limb Prosthesis (Ricaurte et al., 2018)

The design of the socket plays a critical role in achieving a functional and comfortable prosthesis, as it is the part that transfers the forces exerted by the body to the prosthesis (Paternò et al., 2018). Accordingly, the main requirements are that the socket should fit comfortably, provide stability and control, and have dispersed load transmission across the stump. In all activities, the TF socket is controlled by the amputee using the remaining hip musculature; consequently, every effort must be made during the design to ensure that these muscles are fully used without causing discomfort to the patient (Radcliffe M.S, 1955). To make the socket as comfortable as possible, the pressure from the socket should be distributed as evenly as possible over all pressure-tolerant areas (Fergason & Smith, 1999). The distribution of load over a larger surface will decrease the pressure on the limb and improve comfort for the prosthesis user. Certain areas of the stump are considered pressure-tolerant, whereas other areas are very sensitive and should not experience any pressure. Pressure-sensitive areas will turn red when pressure is applied, and the appearance of skin breakdown is highly probable, whereas tolerant areas will only turn red but subside when the prosthesis is removed. The diagrams in Figure 2.2 indicate the pressure-tolerant and –sensitive areas of a TF stump.

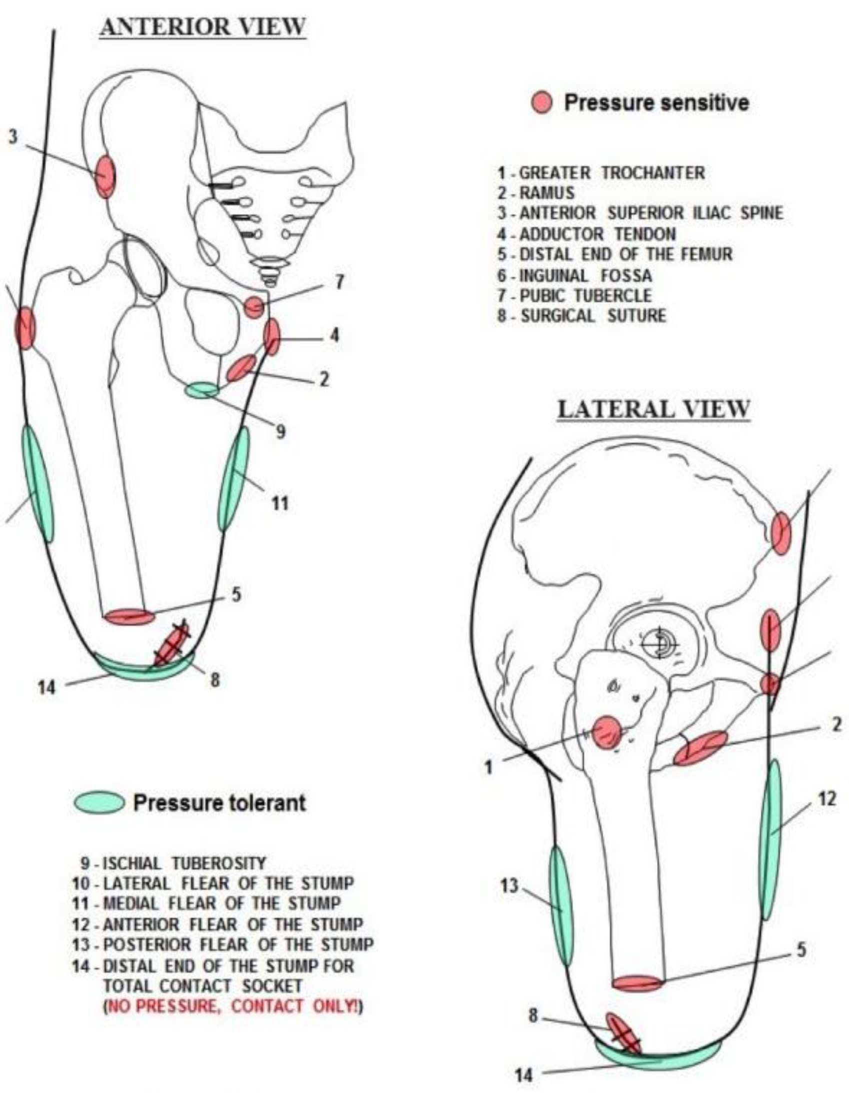

Figure 2.2: Pressure Sensitive and Pressure Tolerant Areas of the TF Stump (Physiopedia, 2022)

Other important design factors of a prosthetic socket include the support system and suspension system. The support system of a socket refers to the weight distribution mechanism, while the suspension system is the mechanism that keeps the socket attached to the residual limb.

2.2.1 Support system

The support system directly influences the fit of the socket, making it a crucial design factor in terms of comfort. The two support systems used in the industry, shown in Figure 2.3, are the ischial containment and quadrilateral sockets. The quadrilateral socket provides support for weight-bearing at the ischial tuberosity on the posterior shelf. The ischial containment socket supports the weight bearing all over the inner surface of the socket, evenly distributed. In this case, the ischial tuberosity does not experience direct weight bearing (Physiopedia, 2022).

Figure 2.3: Quadrilateral and Ischial Containment Support System (Physiopedia, 2022)

2.2.2 Suspension system

The suspension system is the mechanism that prevents the prosthesis from falling off when lifting the leg or during gait. The prosthesis suspension system is a crucial factor in the design as it plays a critical role in energy transfer, comfort, and control of the prosthesis. A poor suspension system will cause friction, which causes skin breakdown and poor control of prosthesis movement. Different suspension systems are available, such as straps, pin and lock, suction with and without liners, vacuum-assisted suspension, and osseointegration (Waihanga, 2022). The commonly used silicone liner and double socket enhance the comfort, function, cushioning, skin protection, and quality of the suspension, superior to other prosthetic suspension systems (Gholizadeh et al., 2014).

2.3 Prosthetic Socket Manufacturing

The manufacturing process of the socket is a critical component in the process of creating successful prostheses. Traditional prosthetic socket manufacturing includes plaster casting and composite lamination. More recently, AM has been introduced to socket manufacturing. Figure 2.4 provides an overview of the steps involved in the respective workflows. Apart from smaller differences in the respective workflows, the AM workflow requires one less step, which involves significant manual labour.

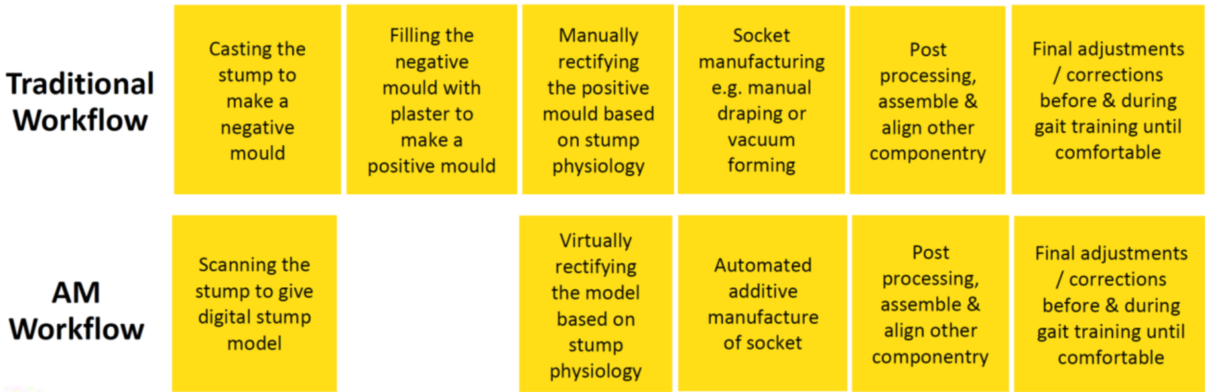

Figure 2.4: Comparison of Prosthesis Manufacturing Workflows (adapted from (Oldfrey et al., 2020))

The first phase in traditional manufacturing of a prosthetic socket is ensuring a secure and comfortable fit through numerous visits to the prosthetist. In the first step, the prosthetist creates a negative cast of the stump and fills it with plaster to create a positive mould of the stump. Through a process called rectification, the positive mould is modified to optimise the fit of the socket. Before creating the definitive socket, a check socket is usually fabricated from a sheet of thermoplastic. Making the check socket transparent allows the clinician to have a complete view of the fit to plan adjustments. After the patient has fitted the check socket, adjustments are made to the positive mould of the stump, which will be used for manufacturing the definitive socket. Multiple fits and adjustments may be required to ensure the best possible design for the most comfortable and effective fit. After the fit has been optimised, the definitive socket can be made. The traditional manufacturing method of definitive prosthetic sockets consists of lamination with carbon fibre and resin (Engstrom & Van de Ven, 1999). Carbon, being highly rigid with a good strength-to-weight ratio, is ideal for the application of prostheses. The disadvantage of its high rigidity, however, is that it causes brittleness and as a result, low impact resistance (Abdulrahman et al., 2021). Additionally, carbon fibre and resin are expensive materials, and the nature of the manufacturing process unavoidably results in significant material waste (Isa et al., 2022). The process is also labour-intensive, depending greatly on the availability, skills and expertise of the prosthetist (Normann et al., 2011). With the focus of the study being on the workflow of creating a prosthesis by AM, a more in-depth review of the AM workflow is required.

2.3.1 Additive Manufacturing Workflow

An AM workflow consists of fewer steps than the traditional workflow. The process starts by 3D scanning the stump to obtain a digital model. 3D scanning has made a digital 3D model of the patient's stump possible through anatomic surface scanning. The scan is used to create free-form three-dimensional data in a triangle mesh or point cloud. The image or scan taken is formatted into a standard reference system and merged to form a complete model (Haleem & Javaid, 2019). A 3D scan normally takes less than 5 minutes to complete, depending on the scanned model size and detail, and provides mesh data for creating an accurate 3D model of the scanned object. 3D laser scanners using triangulation can have an accuracy of up to tens of micrometres (Ebrahim, 2015). Advantages of the 3D scanning method are the accuracy with which the geometry of the stump is captured, the digital format which can be easily stored and reused if needed in the future and the non-contact nature of the process. If preferred, the prosthetist can make a mould of the patient's stump as usual and then 3D scan the mould to be able to capture a digital model as well. There are some challenges involved with using scanning compared to traditional mould making. The stump hanging loose when scanning will have to be overcome by applying pressure with bandages or a compression sock. Alternatively, modifications can be made to the digital model of the stump in the software environment to combat this effect. Cost-effective scanning and modelling methods are crucial for data acquisition and 3D reconstruction to fabricate prostheses by 3D printing. High-quality 3D scanners are generally quite expensive, but modern smartphones are equipped with 3D structured light scanners, which also makes it possible to use them in the application of scanning limbs for prosthetics (Pribanić et al., 2016). The light detecting and ranging (LiDAR) sensor on iPhone models from 2021 onwards has a range accuracy of up to <1mm with close scans (Vogt et al., 2021). The digital model can be stored on a computer's hard drive or in the cloud, reducing the need for physical storage space or manufacturing materials to create a physical model of the stump. A digital model also unlocks the possibility of sharing the file with a prosthetist or designer anywhere in the world if the design and rectifications are not done on-site.

After 3D scanning, the socket can be designed from the scanned geometry utilising 3D modelling software, enabling design and rectifications to be done virtually with great precision and control. Again, if the design of the socket was not done on site, the virtual nature of the process enables the ability to share the digital design file with the manufacturing site from anywhere in the world with internet access. The socket can be produced using AM without the need for manual labour from a prosthetist. After manufacturing by FDM, little to no post-processing is necessary for rounding off the manufactured part. Post-processing of parts manufactured by FDM usually includes removing support prints or trimming away any excess material by hand.

Thereafter, the socket can be bolted to the adapter, which enables connection to the rest of the prosthesis. After assembly of the prosthesis, it is ready for fitting. If rectifications are needed after fitting, the virtual model can be edited, and a rectified socket can be manufactured in a relatively short time. The main advantage of the AM workflow is lower costs because of lower material costs and waste compared to carbon fibre lamination. Additional advantages include the workflow requiring less manual labour and more precise control over design and modifications. The digital nature of this workflow also has the potential to provide prosthetic socket designs to remote locations with access to AM hardware but a lack of expertise.

2.4 Additive Manufacturing

AM is catalogued into seven groups according to ISO/ASTM 52900:2021, including binder jetting, directed energy deposition, material extrusion, material jetting, powder bed fusion, sheet lamination and vat photopolymerization (ISO52900, 2021). The category of material extrusion includes FDM of thermoplastics. FDM is the most commonly used AM method in prosthetic socket research due to its affordability and accessibility (Oldfrey et al., 2020). FDM was a patented term by Stratasys until 2009; fused filament fabrication (FFF) is used interchangeably, as it refers to the same technology (Jones et al., 2011). For consistency, the term FDM will be used in this study, except when referring to studies that use FFF.

FDM is used to create physical objects from a geometric representation, like a CAD model, by successive addition of materials (Shahrubudin et al., 2019). A computer-controlled printer head takes in the thermoplastic material, heats it to a fusion state, and deposits the filament stream in a thin layer onto the printing bed or the previous layer thereafter (Haghsefat & Tingting, 2020). The use of FDM allows the manufacture of customised products that meet individual needs resulting from the specific anatomy of the patient (Jamróz et al., 2018). This, in conjunction with lower tooling costs, makes FDM a suitable manufacturing process for creating prosthetic sockets based on 3D scans. For this specific application, the material to be considered must have a high yield strength to withstand loading conditions and good printability to ensure ease of manufacturing. Fibre reinforcement of polymeric materials has also been shown to significantly enhance mechanical properties. The reinforcement of polymers with short-fibres results in moderately improved mechanical properties of FDM materials, making it a favourable choice for this application (Tekinalp et al., 2014). PETG is a more common FDM material available at a low cost. PETG has favourable mechanical properties as it can endure higher peak stress compared to other common materials like polylactic acid (PLA) and acrylonitrile butadiene styrene (ABS) (Nguyen et al., 2025). More specifically, transparent PETG is the most commonly used thermoplastic for check sockets in the traditional workflow, as it can facilitate the diagnostic processes (Kim et al., 2024).

2.5 ISO 10328 Structural testing of lower-limb prostheses

Structural testing plays a vital role in assessing the reliability, durability, and safety of prosthetic sockets, ensuring that they can endure the mechanical stresses encountered during daily use. This testing is crucial for prosthetic devices, first to ensure user safety and, second, to foster confidence and trust in the device.

No standard for the manufacturing of sockets or mechanical testing is universally accepted. Consequently, prosthetic fabrication facilities use a wide range of materials and procedures, heavily relying on human judgement and operations, which impacts the socket strength (Graebner & Current, 2007). The International Organisation for Standardisation (ISO) standard 10328 was developed as a guideline for the design and testing of lower limb prosthetic components. Incorporating ISO 10328 guidelines into prosthetic design and evaluation processes can be advantageous to ensure the reliability and efficacy of the device. A systematic review by Gariboldi et al. (2022) on structural testing of the lower limb prosthetic socket concluded that ISO 10328 is a viable starting point to define a test guideline. The review investigated studies that reference ISO 10328:2016 and how the standard was adapted for the testing of TT sockets. Owen & DesJardins (2020) found the ISO 10328 testing standard sufficient to complete their evaluations but noted that the method lacks some socket-specific measures and loading conditions that could improve comparisons between different socket types.

2.5.1 Application of ISO10328

Procedures for static and cyclic strength testing on lower limb prosthesis are specified by ISO 10328:2016, where mainly compound loadings are applied as a single test force. The compound loads in the test sample relate to the peak values of the components of loading that normally occur at different instants during the stance phase of walking. The various phases of walking are presented in Figure 2.5. Loading conditions [I] and [II] of ISO10328 correspond to the heel strike and toe-off phase, respectively.

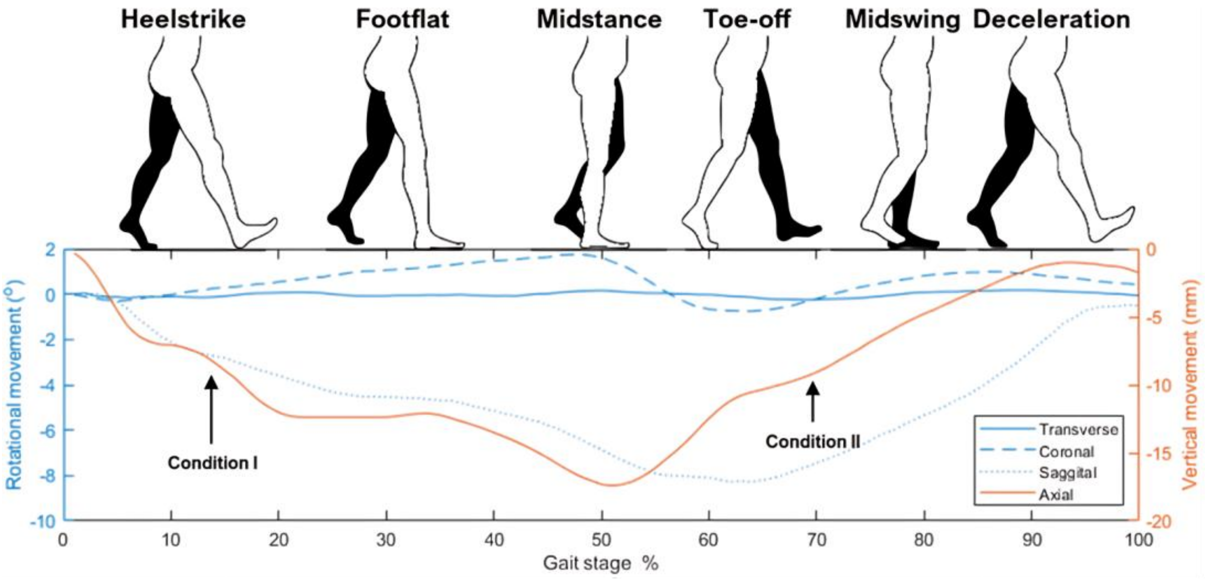

Figure 2.5: Relative femoral movement during the gait cycle of a right transfemoral amputee (Marinopoulos et al., 2023)

The forces applied at these respective phases of walking are prescribed by ISO10328 based on data acquired and classified by body mass for different test loading levels, as shown in Table 2.1 below. Test loading level P5 is based on data from all amputees, including a few whose body mass exceeded 100kg (ISO10328, 2016).

Table 2.1 ISO10328 Test Loading Levels

Test Loading Level	Body Mass [kg]
P3	< 60
P4	< 80
P5	± 100
P6	< 125
P7	< 150

The coordinate system with reference planes for a visual representation of the loading locations and directions, as prescribed by ISO 10328, is shown in Figure 2.6. Focussing on the right leg (1), shown in blue, the only applicable reference planes to a TF socket are the top (3) and knee (5) reference planes (pink). Their respective heights from the bottom reference plane are denoted by u_T and u_K, shown in yellow. Most importantly, points P_T and P_K, shown in green, represent the top load application and knee load reference points, respectively. The offset of point P on each reference plane is governed by entities o and f. Note the entity F_T (red), which depicts the load applied at P_T on a load line passing through P_K. The direction of the load is presented by the load line (4), shown in orange.

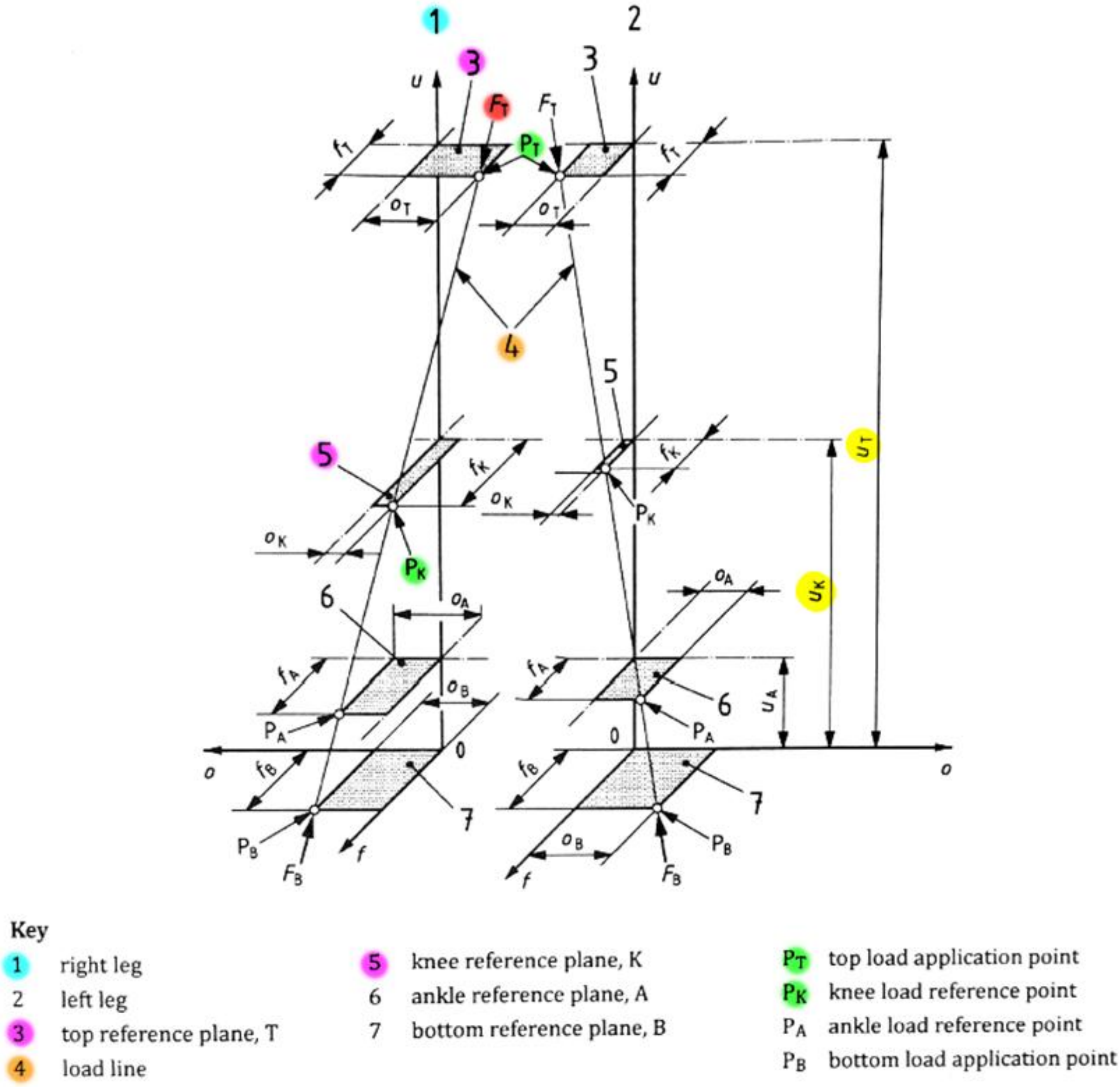

Figure 2.6: Specific configuration showing coordinate system with reference planes (ISO10328, 2016)

In the case of the top reference plane at height u_T not being high enough to accommodate the prosthetic socket, a new top reference plane u_X must be created. Offsets o_X and f_X at height u_X can be calculated by using Equation 1 and Equation 2 prescribed by ISO 10328:

$$\boldsymbol{f_X = f_K + \left\{\frac{(f_K - f_A)(u_X - u_K)}{(u_K - u_A)}\right\}}$$ Equation 1

$$\boldsymbol{o_X = o_K + \left\{\frac{(o_K - o_A)(u_X - u_K)}{(u_K - u_A)}\right\}}$$ Equation 2

Shown in Figure 2.7, Skoglund (2015) tested an additive-manufactured TT socket, made from titanium alloy (Ti6Al4V), according to ISO 10328 loading condition P5 [II]. Steel plates with holes representing the offsets calculated by Equation 1 and Equation 2 connect the socket and pylon to the test bench in conjunction with ball joints.

Figure 2.7: Test rig for TT socket in accordance with ISO 10328 (Skoglund, 2015).

2.5.2 Implementation of ISO 10328 in FEA

During design, ISO 10328 test conditions can be replicated using FEA software to refine the design and evaluate various loading conditions to identify the worst-case scenario. Implementing FEA in this manner reduces the number of specimens to be manufactured and tested, ultimately saving time and cost. FEA has proved effective in analysing prosthetic sockets and in parametric analysis, investigating the effects of various parameters related to socket design, i.e., material properties and thickness (Lenka et al., 2011).

The application of FEA on prosthetic sockets created by FDM, however, presents several challenges. A literature review by Paul (2021) identified several key limitations and research gaps in the application of FEA to FDM-manufactured components: First of all, there are limited studies examining the impact of surface quality and geometric errors inherent in the FDM process on part performance, and these issues are not well captured in current FE models. Factors such as build orientation, loading direction, and layer thickness significantly impact failure mechanisms in FDM parts, but are oversimplified or excluded in simulations. The effects of porosity and internal air gaps are not sufficiently captured, which have a major impact on mechanical behaviour. Thermal stresses are also present due to the transient thermal nature of the FDM process, creating the need for more thorough thermal-mechanical coupling in simulations. Finally, the majority of current FE studies on FDM-manufactured components focus on thermoplastics, not including reinforced or composite filaments, despite their increasing relevance.

2.6 Previous work on additive-manufactured prosthetic sockets

Several studies have investigated the use of different AM technologies and materials for manufacturing prosthetic sockets and their feasibility.

Graebner & Current (2007) used static loading conditions modified from the ISO 10328 test framework to examine the structural performance of different distal pylon-to-socket attachment systems in transtibial composite sockets. Failures consistently occurred at the adapter interface rather than within the socket wall itself. Still, the majority of attachment configurations tested passed the strength component of the standard, especially when carbon-fibre reinforcement was used, according to the study. These findings underscore the significance of joint design and reinforcement strategy for the overall integrity of prosthetic sockets, as well as the attachment mechanism's role as a critical structural vulnerability in socket assembly.

Gerschutz et al. (2011) measured the static failure loads of prosthetic sockets using a modified ISO 10328 for use on three different prosthetic socket types: check sockets, copolymer sockets, and definitive laminated sockets. Their findings demonstrated that wall thickness, material choice, and fabrication method all affected the strength of check sockets made from PETG. In contrast, copolymer sockets showed a comparable dependence but consistently failed the ISO ductile-loading test. This indicates significant variability in socket performance and highlights the need for standardised testing across clinics. In contrast, definitive laminated sockets showed better strength behaviour, but they still varied significantly between fabrication facilities and frequently failed to meet the ISO brittle-loading criterion.

van der Stelt et al. (2022) conducted a study to evaluate the mechanical performance of low-cost, 3D-printed transtibial prosthetic sockets produced using FFF. The research aimed to assess the suitability of various printing materials by conducting tensile tests in accordance with ISO 527 standards. Among the materials tested, Tough PLA emerged as the most suitable due to its favourable mechanical properties and cost-effectiveness. To ensure the structural integrity of the 3D-printed sockets for patient use, the study performed mechanical testing following the ISO 10328 standard, which specifies requirements and test methods for lower-limb prostheses. The Tough PLA socket withstood a static load of 4025 N and completed 2.27 million cycles under dynamic loading conditions without failure. These results indicate that FFF using Tough PLA can produce transtibial prosthetic sockets that almost comply with international structural testing standards. The study concluded that with further research to optimise materials, print settings, and socket design, FFF has the potential to be a viable method for producing low-cost prosthetic sockets, particularly beneficial in resource-limited settings.

Marinopoulos et al. (2023) conducted an experimental investigation into the structural integrity of 3D-printed above-knee prosthetic sockets designed for paediatric applications. The study utilised FDM to fabricate sockets using two materials: polylactic acid (PLA) and carbon-fibre reinforced nylon. These materials were selected for their accessibility and mechanical properties suitable for prosthetic applications. To evaluate the mechanical performance, a custom testing rig was developed in accordance with ISO 10328, replicating the loading conditions experienced during the early stance phase of gait. The sockets were tested under static compressive loads using a silicone-rubber phantom limb that resembles the mechanical properties of human tissue. The load requirements were recalculated to correspond to a 14-year-old male at the 98th percentile for weight, ensuring the relevance of the testing conditions to the target paediatric population. The results demonstrated that, following initial design optimisations, the 3D-printed sockets could withstand loads up to five times the user's body weight without failure. This indicates that FDM-fabricated sockets using PLA and carbon-fibre reinforced nylon possess sufficient structural integrity for paediatric use, offering a promising alternative to traditional manufacturing methods. The study highlights the potential of AM to produce cost-effective, customizable prosthetic sockets suitable for paediatric patients.

2.7 Summary

The literature review established the fundamentals of transfemoral prosthetic socket design, highlighting the significance of efficient load distribution, user comfort, and control, supported by knowledge of pressure-sensitive and pressure-tolerant areas. An additive manufacturing workflow, which combines 3D scanning, CAD design, and FDM fabrication, offers greater affordability, efficiency, design control, and opportunities for remote clinical support, while traditional manufacturing methods are labour-intensive, time-consuming, and expensive. ISO 10328, as a testing standard, was investigated, along with its loading conditions, test setup, and applicability to both simulation-based and physical design evaluation. An overview of earlier research on additively manufactured prosthetic sockets was presented at the end of the chapter, emphasising current developments and highlighting the need for more research.

CHAPTER 3: METHODOLOGY

3.1 Introduction

The methodology employed a structured approach covering the design, simulation, and testing phases. The process started with 3D scanning and digital reconstruction of an existing transfemoral socket, followed by design development of two socket designs. FEA simulations were conducted for design selection and experimental validation of the final design for compliance with ISO10328. The workflow used in the study is summarised and illustrated by the flowchart shown in Figure 3.1.

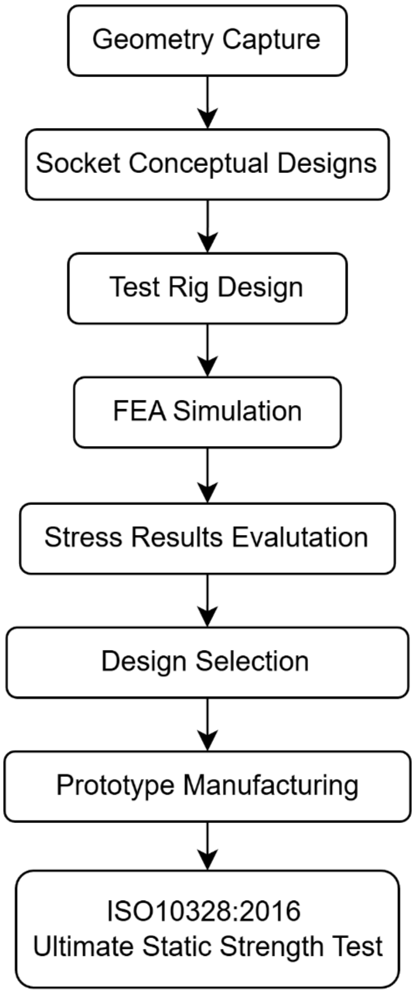

Figure 3.1: Methodology Flowchart

3.2 Geometry Capture

3.2.1 3D Scanning

An existing TF check socket was 3D scanned to obtain a digital copy for designing the prosthetic socket prototypes. Using an existing socket rather than scanning the residual limb of an amputee eliminated the need for a qualified prosthetist or invasive interaction with an amputee. The setup of the 3D Scanning process is shown in Figure 3.2a. The scanner was connected to a computer to process the scan data and save the point cloud data. The handheld scanner used was the EinScan Pro HD from SHINING 3D, shown in Figure 3.2b. In Handheld Rapid Scan mode, the scanner had an accuracy of up to 0.1 mm. The socket was spray-painted as it had transparent surfaces, which proved difficult to scan (Figure 3.4c). Marker stickers also improved the ability of the scanner to map the scanned surfaces accurately as it moves around the object (Figure 3.2d).

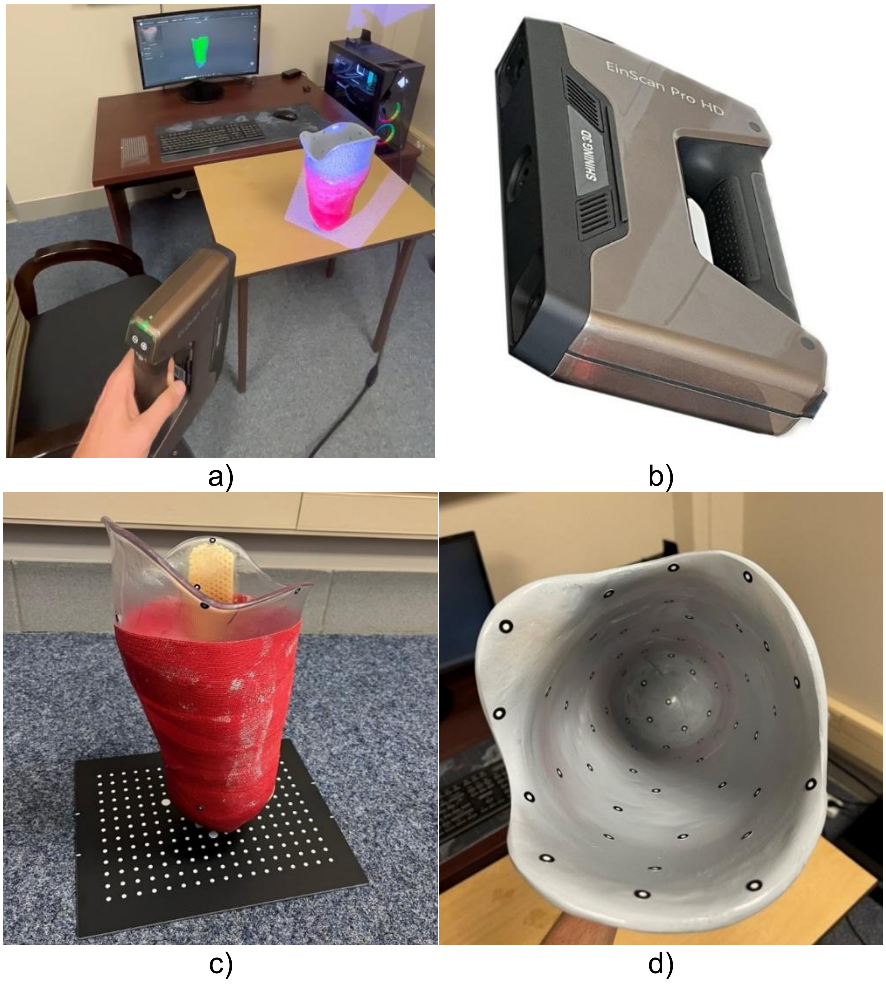

Figure 3.2: a) 3D Scanner and PC setup; b) EinScan Pro HD from SHINING 3D; c) Transparent socket before painting; d) Painted inside socket with marker alignment.

Only the inner surface was used in the prototype design, but scanning the entire socket was necessary to ensure the adapter of the prototype socket is accurately aligned according to the check socket created by a qualified prosthetist. This ensured the prototype conforms to the measurements and alignment of the prosthetist. Detecting the deepest part of the inside surface proved challenging, as the socket was narrow and deep. Extra care was taken to scan the deepest part and ensure the geometry is captured as completely as possible. Any small missing surfaces were filled in afterwards using repair tools in the post-processing software. A smaller scanner would be advantageous in this regard. After scanning, some postprocessing was done before the inside surface scan was usable in the CAD design.

3.2.2 Scan post-processing

Some basic postprocessing was done in the native scan processing software of the scanner, EXScan Pro, before exporting the point cloud file to an OBJ file, which is a common mesh file type. Cleaning up the scan involved removing any unwanted surfaces, which also reduced the file size and made the processing of the file easier for the computer when editing the scan data. The triangle count was reduced to lower the mesh quality to an acceptable level regarding the physical size, which further improved the speed of processing the file.

More specialised mesh editing software was needed before the scanned geometry could be used in the CAD design. MeshMixer from Autodesk is a free software program that has proved useful as an artistic tool for editing the mesh before importing it into CAD software. The goal of the process was to extract a complete and smooth scanned surface from the inside of the socket. After importing the mesh file into MeshMixer, the scan was aligned with the global coordinate system by using the transform feature, shown in Figure 3.3.

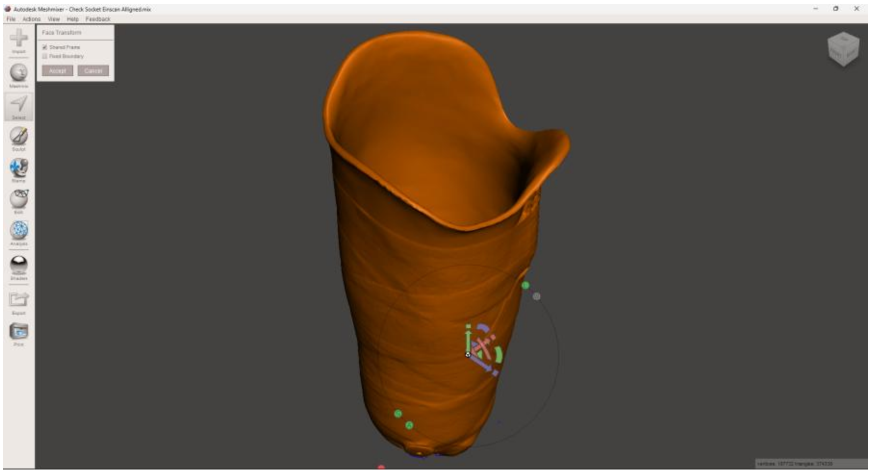

Figure 3.3: Aligning the scan to the global coordinate system.

After aligning the socket, the “Inspector” tool was used to fix any errors in the mesh and close any open surfaces (Figure 3.4a). Selecting the edge between the inside and outside surface of the socket and using the “Smooth Boundary” tool created a split line on the edge (Figure 3.4b) to separate and extract the inside surface of the socket (Figure 3.4c). The last step was to smooth the inner surface to make the conversion to a CAD surface as easy as possible (Figure 3.4d).

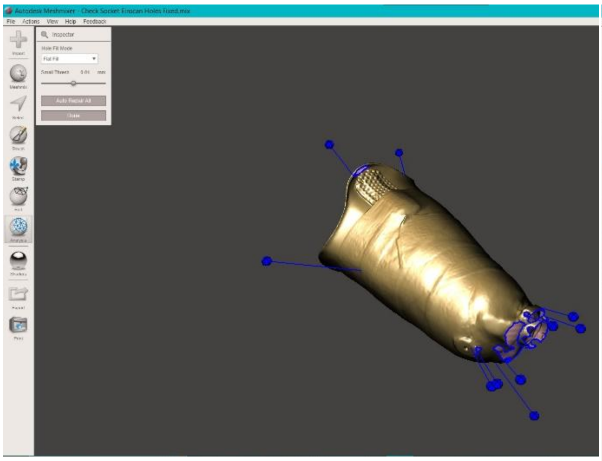

a)

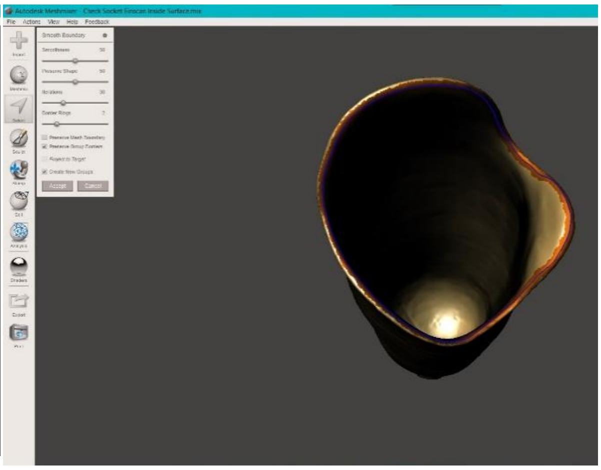

b)

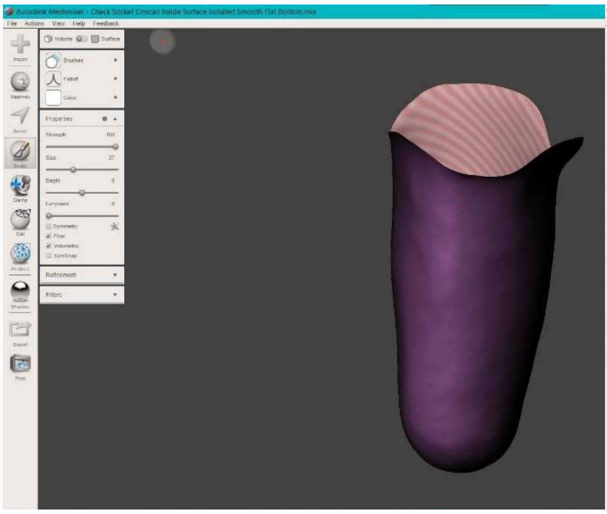

c)

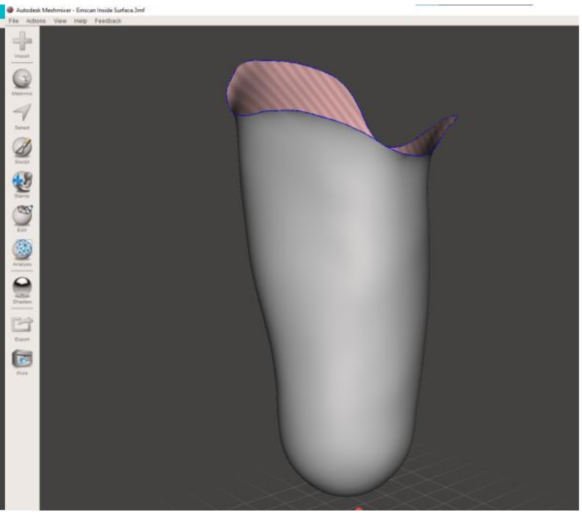

d)

Figure 3.4: a) The inspector tool is used to identify all holes; b) A Smooth boundary feature is applied to the edge to split the inner surface from the socket; c) The inside surface of the socket is extracted and isolated; d) The extracted inside surface is smoothed.

After extracting the smoothed inside surface of the socket, the file was saved as an STL file, which is a common mesh file type, compatible with being imported into most CAD software.

3.3 Conceptual Designs

Two conceptual designs were developed using the same stump geometry, differing primarily in the attachment mechanism at the distal end. The CAD designs of the sockets were done in SolidWorks. The STL file of the 3D scan was imported using the ScanTo3D tool in SolidWorks and converted from a mesh body into a surface body, as shown in Figure 3.5.

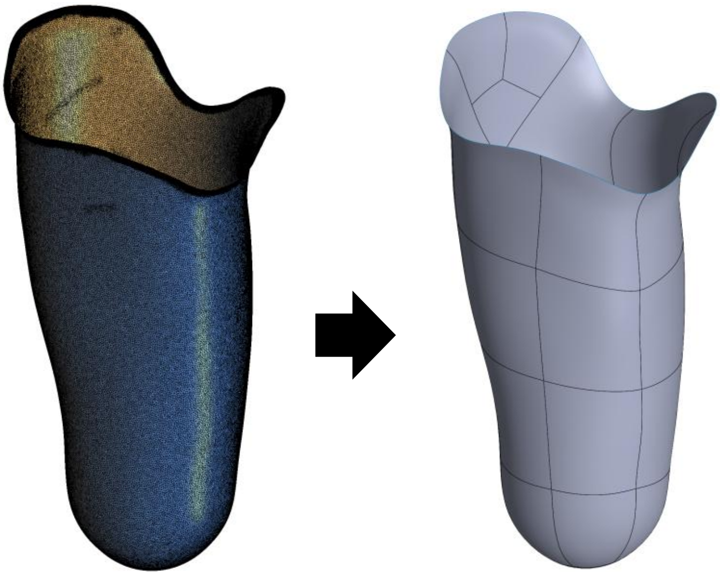

Figure 3.5: Mesh conversion to BREP surfaces using SOLIDWORKS ScanTo3D.

From the surface body in SolidWorks, both a stump and a socket were modelled with surface modelling. For the socket, a conceptual design was needed which could be refined after FEA. The main parameters of the design included the socket thickness and geometry of the distal end of the socket, which refers to the region where the socket attaches to the rest of the prosthetic limb. The distal end was designed to be compatible with the standard 4-hole pyramid adapter, as shown in Figure 3.6. Accordingly, the distal end was designed with four M6 holes with a spacing of 35 mm.

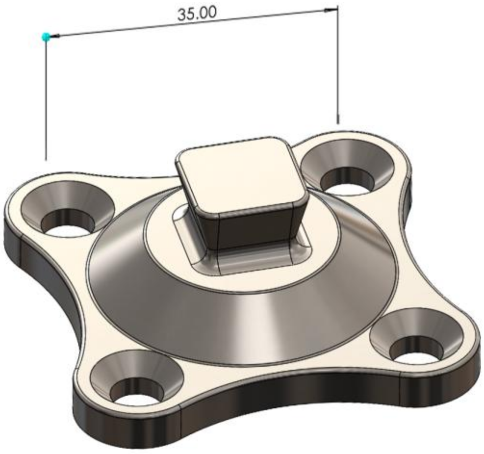

Figure 3.6: 4-Hole Male Pyramid Adapter

In MeshMixer the adapter at the distal end was measured from its centre to the origin in the X and Y direction. Accordingly, the design of the adapter attachment area was offset from the origin to correspond to the original alignment as measured and specified by the prosthetist on the scanned check socket, as shown in Figure 3.7.

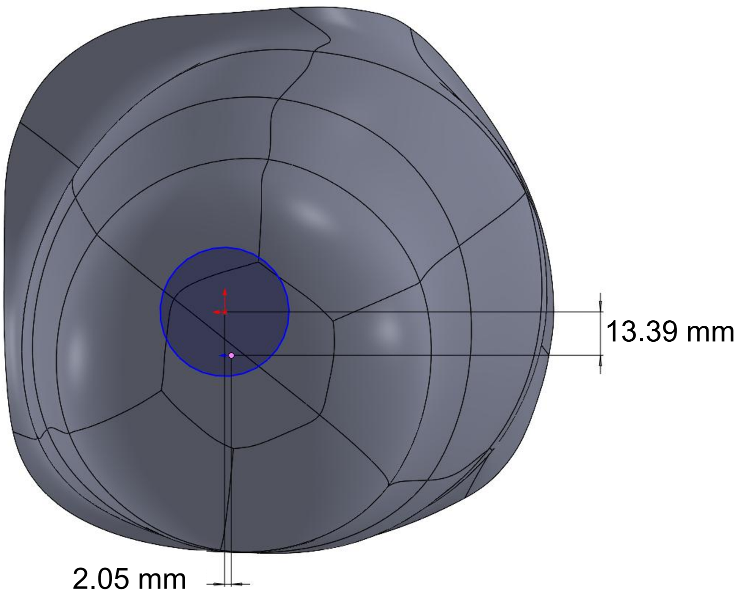

Figure 3.7: Location of adapter centre as measured from origin.

3.3.1 Socket Design 1

After the adapter attachment surface was created, the socket was thickened by 4 mm to form a solid body from the initial surface (Figure 3-8a). The outer surface of the socket was cut with a split line to merge the thickened socket with the planar adapter surface (Figure 3-8b). The resulting surfaces were then connected using a lofted surface with tangent start and end conditions, ensuring a smooth geometric transition (Figure 3-8c). Once the geometry was watertight, the surface body was converted to a solid. Circular cut-extrudes were added to create blind holes for dowel nuts, followed by four M6 holes extending from the adapter's planar surface to the cut-extrudes to allow fixture of the pyramid adapter using countersunk screws and dowel nuts (Figure 3.8d).

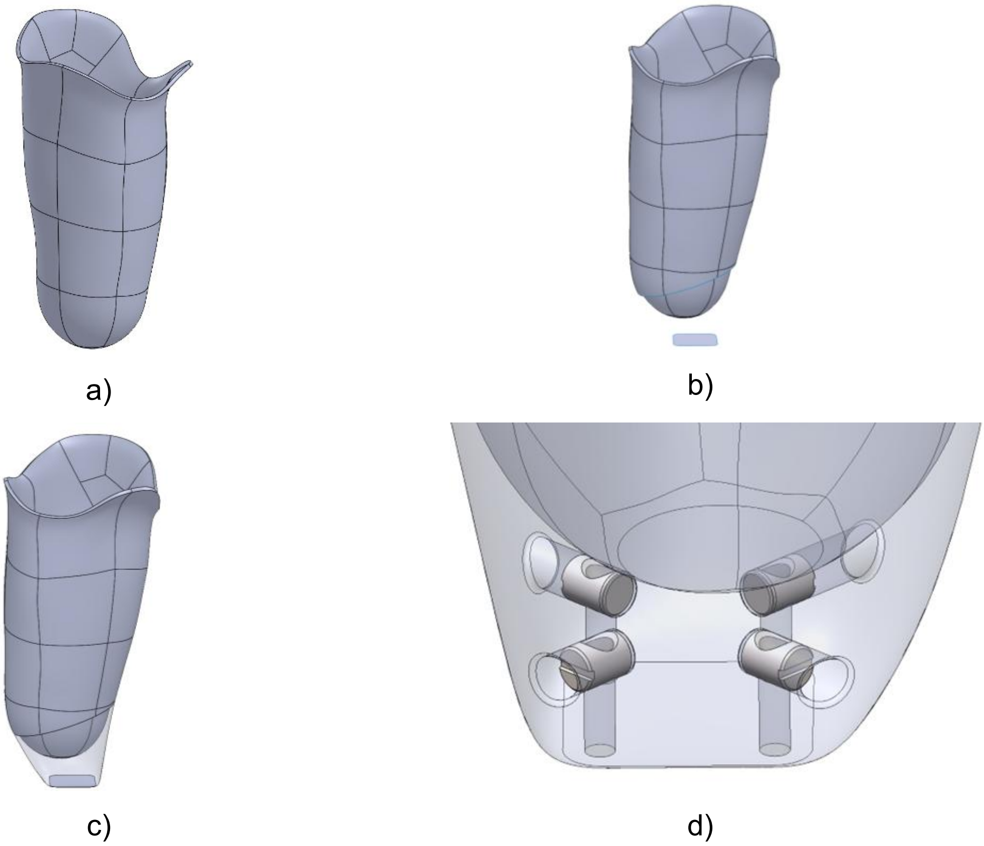

Figure 3.8: a) Surface thickened to 4mm; b) Split line cut outer face of socket; c) Lofted surface to merge thickened socket with the planar adapter surface; d) Circular cut-extrudes to facilitate fasteners.

These steps produced a TF socket design, excluding a suspension system, that was suitable for FEA and design optimisation. The completed Socket Design 1 is shown in Figure 3.9.

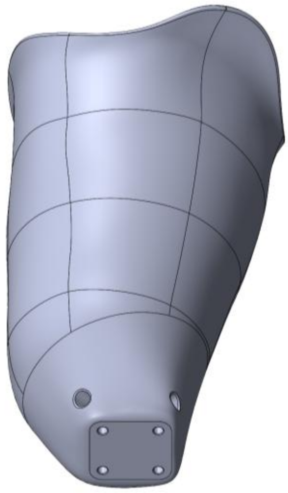

Figure 3.9: Completed Socket Design 1

3.3.2 Socket Design 2

For Socket Design 2, the attachment area was changed from a square with rounded edges to a circular shape, as shown in Figure 3.10a. The removal of corners was done as far as possible to eliminate stress concentrations. The contact stresses caused by the dowel nuts were of concern, and accordingly, the new design replaced the fixtures with a system that had a more even distribution of force over a larger contact area. The new design, as shown in Figure 3.10b, replaced the dowel nuts with a rounded corner square plate with threaded M6 holes. This change also removed the holes that housed the dowel nuts, which resulted in the removal of material in a critical area. Lastly, a rib was added to the area of the socket, which supports the ischial tuberosity, as shown in Figure 3.10d. This design change was made due to the overhang exceeding 45°, which is likely to experience sagging during manufacturing with FDM. The addition of the rib helped with manufacturability but also strengthened the area of the socket, which supports the ischial tuberosity.

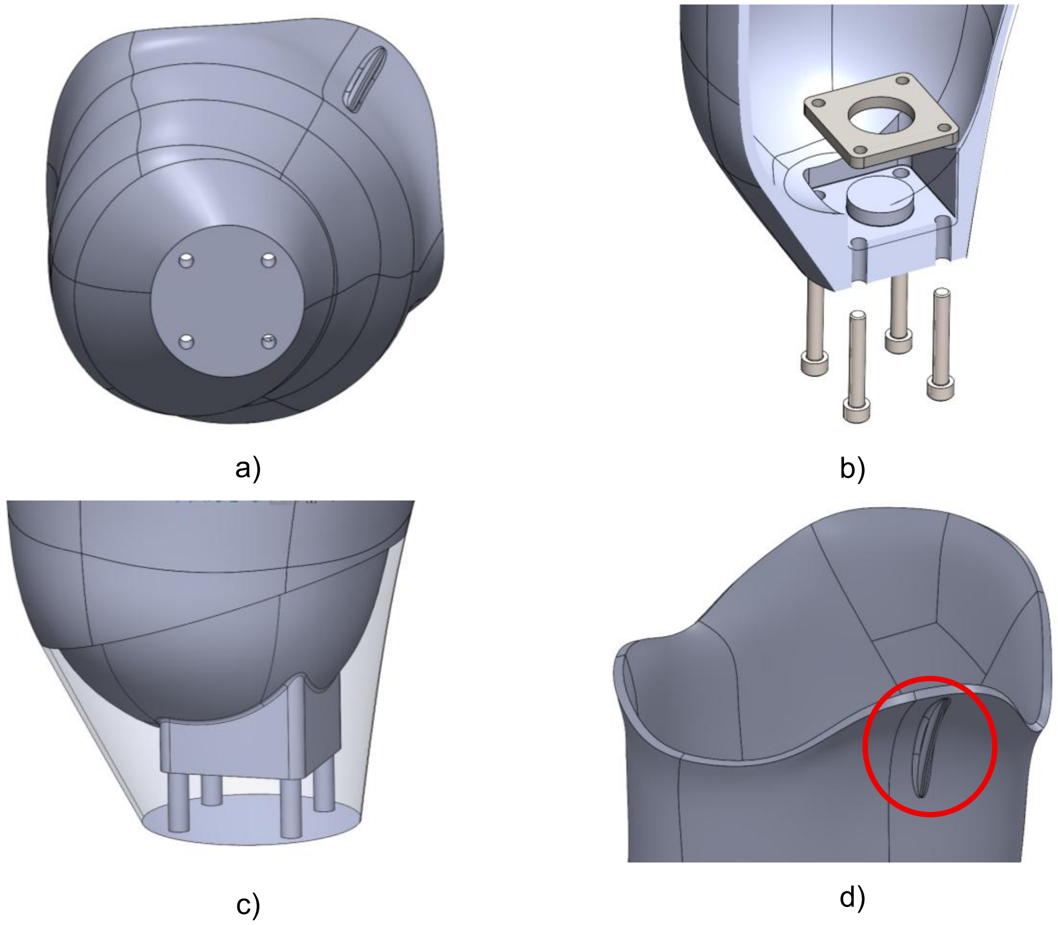

Figure 3.10: a) Circular adapter attachment region; b) Square plate insert with threaded M6 holes; c) Internal geometry of the distal end, Socket Design 2; d) Rib added to the region supporting the ischial tuberosity.

The completed Socket Design 2 is shown below in Figure 3.11.

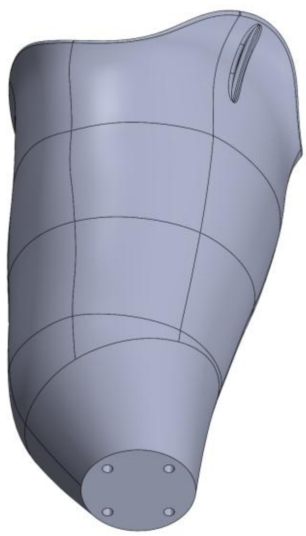

Figure 3.11: Completed Socket Design 2

3.4 Test Rig Design

A test rig was designed to apply the forces and restrain the socket as prescribed by ISO 10328 in the FEA simulation, as well as for final mechanical testing.

First, a CAD model of the stump was needed for the FEA simulation to transfer the exerted force to the socket, as well as a physical model of the stump for final mechanical testing. The CAD model, as represented in Figure 3.12, was designed utilising the same 3D scanned surface that was used for the socket designs.

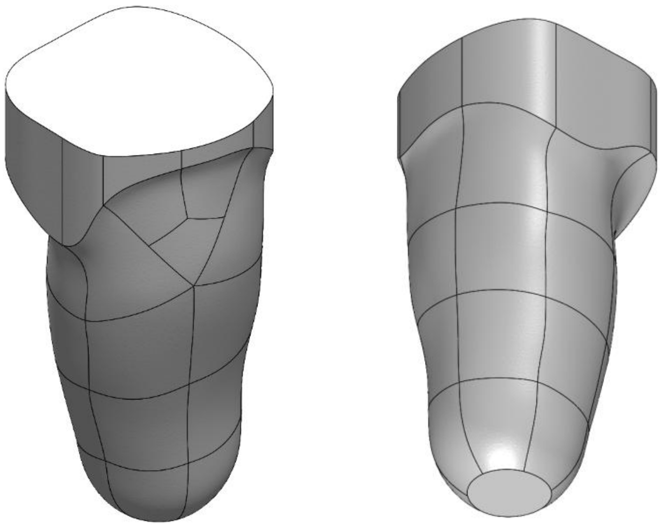

Figure 3.12: CAD model of the stump.

The loading directions and locations prescribed by ISO10328 are discussed in Chapter 2.5.1 . The determined height to accommodate the TF socket was measured to be uX = 940 mm, resulting in a total height of 440 mm for the testing setup from the knee plane uK = 500 mm to uX. Table 2 contains the prescribed and newly calculated reference planes and dimensions of offset locations for loading forces. The formulas that were used for calculating offsets f_X and o_X are defined in the literature review by Equation 1 and Equation 2.

Table 3.1: Reference dimensions for loading forces, directions, and locations.

Reference Plane	Offset Location	Dimensions for Test Loading Level P5 [mm]	
		I	II
Top	u_T	650	650
	f_T	82	55
	o_T	-79	-40
Knee	u_K	500	500
	f_K	52	72
	o_K	-50	-35
X	u_X	940	940
	f_X	140	22
	o_X	-134	-49

The physical manufacturing of the test rig is reported in Testing Rig Manufacturing. After casting, the stump was fitted into the existing check TF socket to ensure it was modelled and manufactured accurately, as shown in Figure 3.13.

Figure 3.13: Casted Stump fit in scanned TF Check Socket

The final design of the complete testing setup can be seen in Figure 3.14a. During the manufacturing of the top plates, a calculation error in the offsets caused inaccurate dimensions of the top plate ordered from the manufacturers. A second top plate was designed and manufactured to correct the error and ensure the loads were applied accurately. The new top plate was bolted onto the existing top plate. Accordingly, new calculations had to be performed to determine the dimensions for the accurate application of the load in accordance with ISO 13028 at the new height, as shown in the ISO 10328 Revised Calculations. The modified setup with the added second plate, which was used for testing, can be seen in Figure 3.14b.

Figure 3.14: Complete Testing Setup (a) CAD Design (b) Modified as built

3.5 FEA Simulation

The application of FEA enabled the identification of high-stress regions on the socket that could be strengthened through design modifications. Given the plastic composition of the socket, characterised by its non-linear properties, and the testing procedure that stressed the socket beyond its yielding point, a non-linear FEA became necessary. The scarcity of comprehensive material data for FDM materials, the isotropic characteristics of FDM-manufactured parts, and the variability of mechanical properties due to manufacturing conditions introduced sources of error and uncertainty. These factors could potentially result in complex, time-consuming simulations with an anticipated low accuracy. Therefore, a simpler linear static FEA was conducted as a comparative analysis among design iterations, utilising material properties obtained from literature for the FDM materials.

3.5.1 Linear Static FEA Setup

The material used for the comparative FEA simulations was PETG. The material properties for the PETG filament, as shown in Table 3.2, were extracted from a study by Huysamen et al. (2020) who obtained the material datasheet from the filament supplier 3D4MAKERS's webpage.

Table 3.2: Material properties of PETG

Material properties	
Elastic modulus	2.2 GPa
Poisson's ratio	0.33
Density	1290 kg/m^3
Yield Strength	47.9 MPa

All FEA studies were conducted as linear static studies in SOLIDWORKS Simulation. The setup was simplified as much as possible to reduce runtimes and prevent errors and run failures due to the complexity of contact interactions or mesh size. The fixtures and loads were meticulously applied to replicate the real-life setup as closely as possible while avoiding excessive fixtures, which would over-constrain the model. Two axes were created in the CAD environment to align with the holes in the top and bottom plates, as shown in Figure 3.15. These axes correspond to the loading line prescribed by ISO 10328 loading conditions P5 [I] and [II].

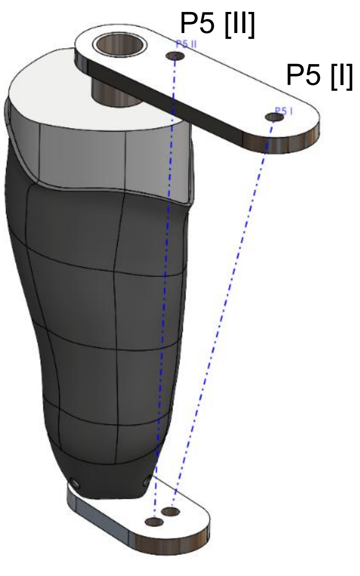

Figure 3.15: FEA Loading Conditions Reference Axes

For simplification purposes and to reduce the runtime of the simulation, some components, such as the top and bottom plates, were excluded from the analysis and replaced with representative boundary conditions. As those parts were involved in transferring loads and are now being simulated as a rigid interaction, it was deemed an appropriate simplification, still providing a conservative result regarding the stress experienced by the socket. The force was applied to the shaft in the stamp as a remote load, which enabled the exclusion of the top plate from the analysis. A load of 4.48 kN in the X-direction of Coordinate System 1 was applied in accordance with loading condition P5 I, as shown in Figure 3.16a. The shaft, as well as the stump, was set as rigid bodies that will not deform under load. This also helped reduce simulation runtime. Other parts replaced with boundary conditions or virtual connectors were the bolts fixing the socket to the bottom plate with dowel nuts. The bolts were replaced with virtual pin connectors, which rigidly connect the cylindrical surfaces (Figure 3.16b). The dowel nuts, however, were included as they play a critical role in the contact stresses developed from their interaction with the socket. A fixed geometry boundary condition was applied to the threaded holes of the dowel nuts (Figure 3.16c). Lastly, the bottom plate was replaced with a rigid virtual wall (Figure 3.16d). This would allow contact stresses to develop on the bottom surface of the socket without the need for meshing and solving the bottom plate.

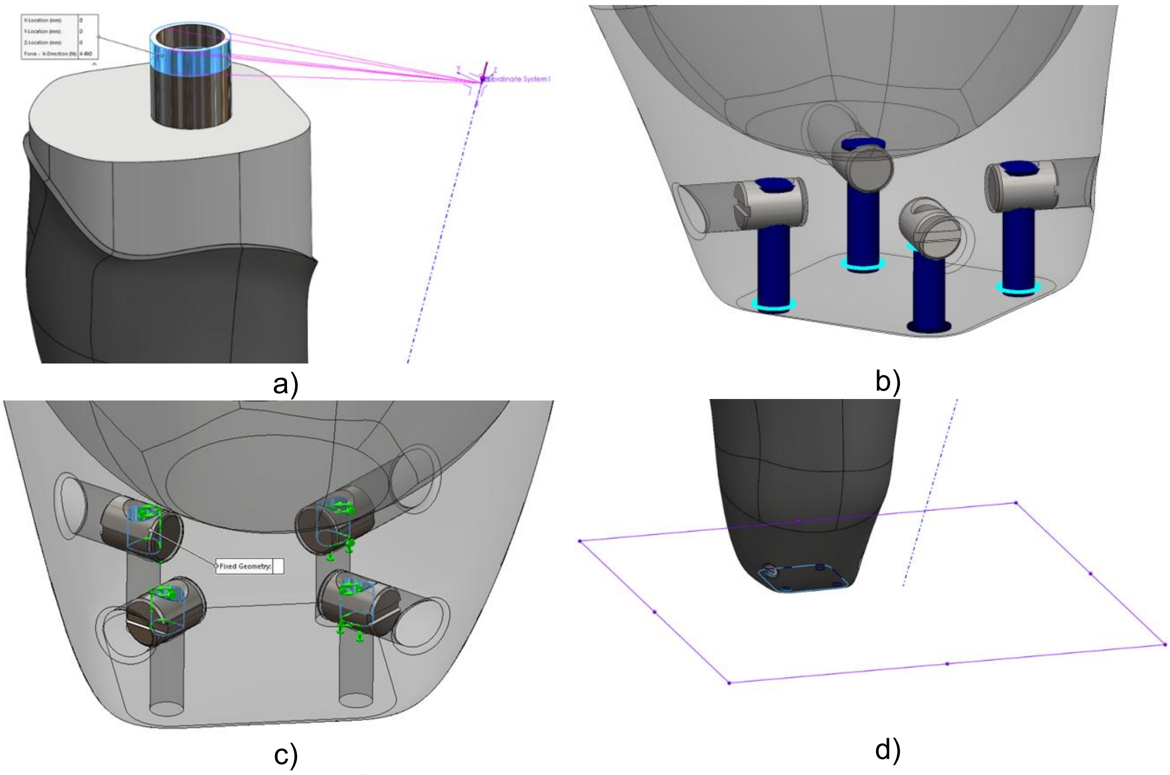

Figure 3.16: a) Remote load definition; b) Virtual pin connectors applied to co-axial M6 holes; c) Fixed geometry applied on the threaded holes of the dowel nuts; d) Socket and virtual wall contact local interaction.

A remote load of 4.48 kN in the X-direction of Coordinate System 1 was applied identically to Socket Design 1, as shown in Figure 3.17a. The shaft and stump were again treated as rigid bodies to ensure consistency in comparison between designs. Other parts replaced with boundary conditions or virtual connectors were the bolts that fix the socket to the bottom plate via four M6 threaded holes in the attachment plate. The bolts were replaced with virtual pin connectors, which rigidly connect the cylindrical surfaces, as shown in Figure 3.17b. A contact interaction was defined between the attachment plate and the socket to simulate the contact stresses that develop during loading. A fixed geometry boundary condition was applied to the threaded holes of the attachment plate, as shown in Figure 3.17c. Lastly, the bottom plate was again replaced with a rigid virtual wall defined on the bottom face of the socket, as shown in Figure 3.17d.

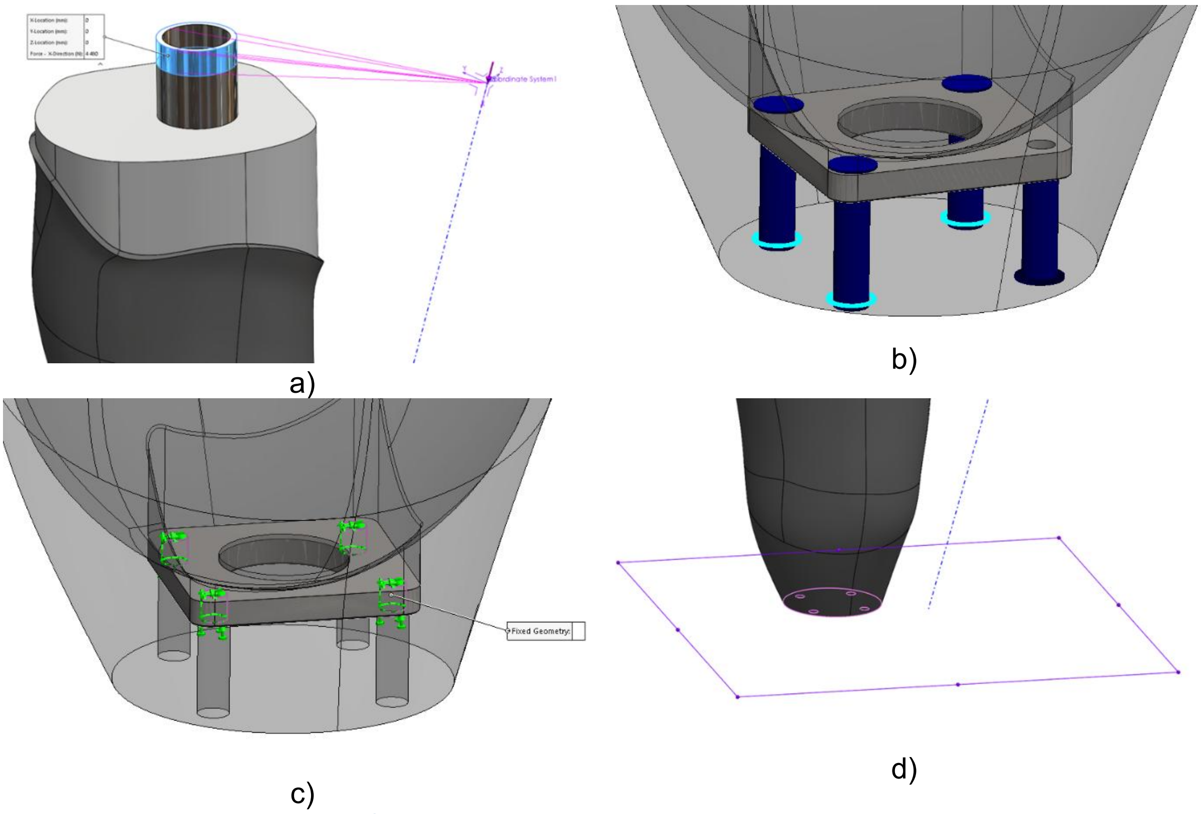

Figure 3.17: a) Remote load definition; b) Virtual pin connectors applied to coaxial M6 holes; c) Fixed geometry applied on the threaded holes of the attachment plate; d) Socket and virtual wall contact local interaction.

Mesh controls specifying an element size of 0.2 mm were applied to the dowel nuts, as well as to the holes of the socket in which they are inserted, as that area was suspected to produce stress concentrations. 0.2mm element size was the smallest mesh size the available hardware could solve before the number of degrees of freedom in the analysis exceeded the hardware's capacity. This would ensure that mesh independence has been reached as far as possible with the available hardware.

3.5.2 FEA Results

As previously noted, the absolute accuracy of the maximum stress values is expected to be low due to the limitations and simplifications outlined. However, as these entities were used for comparison, the absolute accuracy is not a concern. Table 3.3 compares the maximum von Mises stresses of Socket Design 1 and Socket Design 2 under both loading conditions, providing quantitative data for design selection.

Table 3.3: Comparative maximum von Mises Stress Results

Loading Condition	Socket Design 1: Maximum von Mises stress [MPa]	Socket Design 2: Maximum von Mises stress [MPa]	Difference in the Maximum von Mises stress
P5 [I]	261.161	156.168	40.20%
P5 [II]	242.002	140.447	41.96%

Socket Design 2 yielded a significantly lower maximum von Mises stress compared to Socket Design 1. Accordingly, Socket Design 2 was selected for the manufacturing of experimental test specimens. The FEA results also proved that loading condition P5 [I] was the worst-case loading scenario and was accordingly used as the sole loading condition for experimental testing.

3.6 Manufacturing of Test Specimens

A total of five TF sockets were manufactured using a Raise3D Pro 3 Plus printer with a build volume of 300 x 300 x 605 mm. Three were made from PETG, a more common, low-cost material, and two from carbon fibre-infused nylon, a higher-cost, exotic material. The PETG was sourced from SA Filament, and the carbon fibre-infused nylon from eSUN, named ePA-CF (engineered polyamide carbon fibre). Clear PETG was selected to investigate the transparency that could be achieved if the material were to be used for fabricating a check socket, as discussed in Chapter 2.4. Both filaments were dried at 65°C before printing. PETG was dried for 4 hours, and ePA-CF for 12 hours, per the manufacturer's recommendation. The nozzle temperature for PETG was specifically set to the higher end of the range specified by the manufacturer. Higher printing temperatures enhance fusion between printing layers, increasing strength particularly between layers (Hsueh et al., 2021). This also benefits the transparency of the walls when printing with clear PETG. Furthermore, the cooling fan was switched off to further improve interlayer adhesion. The cooling fan was increased to 30% speed to support the overhang angles at the level where the top edge of the socket begins. The printer settings for each material, shown in Table 3.4, correspond to the manufacturer's recommendations for optimal quality and test-prototype strength. Additional printing parameters and slicer settings are included in Appendix D: Socket Manufacturing.

Table 3.4: Printing parameters

Printing parameters	ePA-CF	PETG
Nozzle Diameter [mm]	0.6	0.6
Layer Height [mm]	0.3	0.3
Extrusion Width [mm]	0.7	0.7
Initial Flow Rate	115%	115%
Flow Rate	100%	100%
Wall Count	5	5
Infill	100%	100%
Infill Pattern	Lines	Lines
Nozzle Temp [°C]	260	250
Bed Temp [°C]	100	75
Print Speed [mm/s]	60	60
Cooling Fan	OFF	0% - 30%
Bed adhesion	Brim	Brim
Brim Width [line count]	50	10
Bed Type	Heated Buildtak Bed with PVP Glue	Heated Buildtak Bed

The initial print time for a full socket was predicted by the slicer software to be 36 hours. By varying the extrusion width, the total print time was reduced to 28 hours.

The ePA-CF sockets presented significant manufacturing challenges. Two attempts both failed to complete due to bed adhesion problems. Mitigation strategies employed included printing with an extended brim, increasing the bed temperature, and applying PVP glue to the bed surface. The employed strategies improved but did not fully resolve the adhesion issues. Accordingly, the print was stopped before completion, as shown in Figure 3.18a. Additional complications included the deposition of blobs by the nozzle, shown in Figure 3.18b, producing irregularities in the wall structure, and low dimensional accuracy due to warping. Warping at the distal end caused interference with the attachment plate fit.

Figure 3.18: ePA-CF 1 specimen's defects (a) Incomplete prototype due to bed adhesion failure (b) Nozzle deposition of blobs on outer walls

Given the repeated print failures and the challenges experienced with the ePA-CF filament, manufacturing was halted. As a defect-free ePA-CF prototype could not be produced, the material was consequently not used for testing. Attempting to test defective specimens would not yield a valid comparison with the standard or between the selected materials.

In contrast, the PETG sockets were fabricated successfully without any challenges. The external surfaces of the sockets were uniformly smooth, with the exception of the layer seam, an inherent FDM artefact. Bed adhesion was consistently maintained throughout the entire printing process, and the resulting components exhibited high dimensional accuracy. This dimensional accuracy facilitated an optimal light press-fit of the attachment plate within the socket. A complete PETG prototype is displayed on the print bed in Figure 3.19.

Figure 3.19: Complete PETG TF Socket Prototype

3.7 Structural Testing

An ultimate static strength test was conducted in accordance with the ISO 10328 standard to evaluate the structural performance of the final socket design and the selected materials. The purpose of this test was to determine whether the FDM-manufactured TF sockets could withstand the loading conditions representative of level P5 loading condition [I]. All structural testing was performed on an MTS E45.105 electromechanical universal testing machine, equipped with a 100 kN load cell featuring a measurement accuracy of ±1.0% of the applied force. During each test, compressive force and actuator displacement were recorded continuously.

The loading entities and magnitudes of loading condition P5 [I] were obtained directly from ISO10328 (2016) and are specified in Table 3.5 below.

Table 3.5: ISO 10328 Level P5 Loading Condition [I]

Entity	Abbreviation	P5 [I]
Stabilising test force	Fstab	0.05 kN
Settling test force	Fset	1.024 kN
Static proof test force	Fsp	2.240 kN
Static ultimate test force	Fsu	4.480 kN

The testing procedure followed the sequence prescribed in ISO 10328 for the ultimate static strength test and corresponded directly with the loading curve illustrated in Figure 3.20. The steps executed for each specimen were as follows:

1. Apply F_{set}.
2. Maintain the load for 30 seconds.
3. Fully unload the specimen.
4. Allow the specimen to rest for 10 minutes.
5. Apply F_{stab}.
6. Increase the force at a constant rate of 100 N/s.
7. Stop when F_{su} is reached or structural failure occurs.

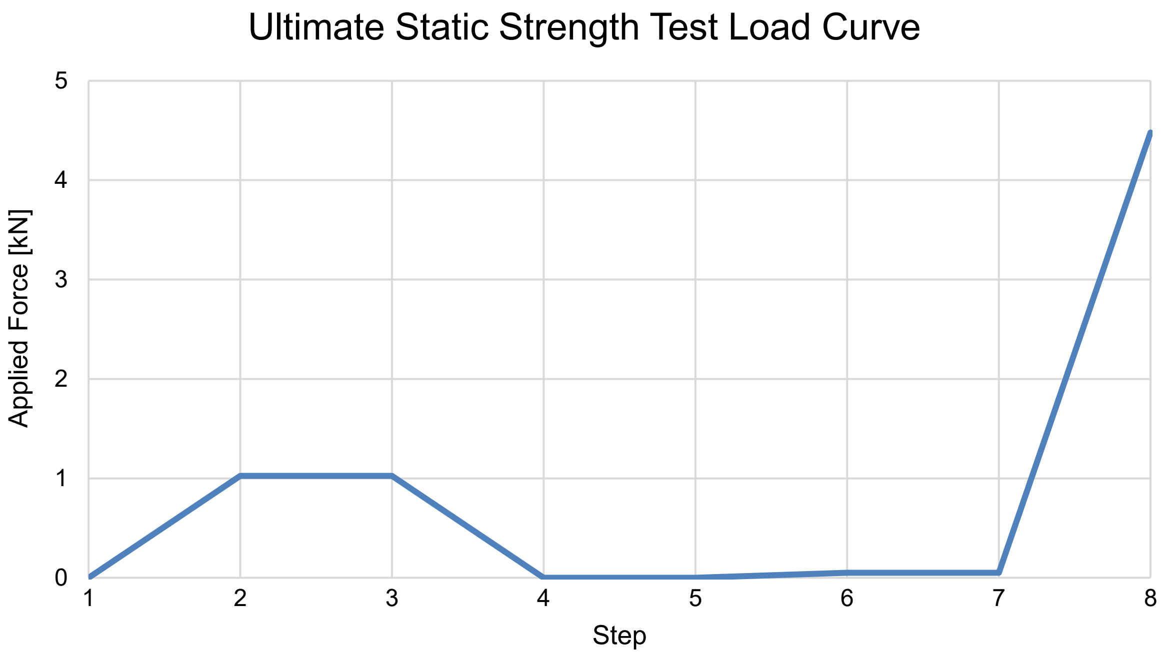

Figure 3.20: Load curve of the ultimate static strength test

The final testing setup, including the test bench, testing rig and a PETG test specimen, is shown in Figure 3.21.

Figure 3.21: Final Testing Setup

Due to the catastrophic failure observed during the first PETG prototype test—where the socket fractured suddenly at approximately 7.2 kN—an adjusted testing strategy was employed for subsequent specimens. Only the first PETG specimen was loaded until complete failure to characterise the failure mode. The remaining PETG specimens were limited to 5 kN, exceeding the ISO ultimate requirement while preventing potential damage to the testing equipment and custom test rig.

3.8 Summary

The methodology followed a structured sequence of well-defined steps. The process began with the 3D scanning of an existing TF prosthetic socket to accurately capture its geometry. The scanned data was then post-processed to repair flaws and prepare the surface for use in the CAD environment. Two conceptual designs were created in SOLIDWORKS, with the main difference being the distal-end adapter interface. The final design was selected based on a comparative linear static FEA analysis. To ensure realistic loading conditions, a test rig was designed in accordance with ISO 10328 for use in simulations and, finally, physical testing. The designed test rig was manufactured and assembled for physical testing in accordance with ISO 10328. Specimens were then fabricated using FDM with two different materials: PETG and ePA-CF. Manufacturing challenges prevented the successful fabrication of defect-free ePA-CF specimens. Consequently, ultimate static strength tests were conducted only on PETG specimens.

CHAPTER 4: EXPERIMENTAL RESULTS AND DISCUSSION

This section presents and discusses the results from the study's experimental phases. The experimental structural testing results validate the design concept, assess material performance, and check compliance with ISO 10328 standards. Load-displacement data collected during testing are shown and analysed. The failure modes are examined and illustrated in figures, with failure locations qualitatively compared to FEA outcomes.

4.1 Results

The load-displacement responses of all PETG specimens showed high stiffness, as shown in Figure 4.1. All specimens met and exceeded the ISO 10328 P5 [I] requirement of 4.48 kN. PETG 1 was loaded to failure at approximately 7.2 kN, where a sharp failure point was observed. This catastrophic failure caused the testing rig to detach at the machine feet parts, but the rig sustained no permanent damage and was repaired for use in subsequent tests. Consequently, PETG 2 and PETG 3 were limited to a maximum loading of 5 kN to protect the rig while still ensuring that the test specimens passed the required 4.48 kN loading level. Furthermore, the slope of the load-displacement graphs for PETG 2 and PETG 3 remained linear up until 5 kN, as shown in Figure 4.1. Accordingly, it was concluded that no permanent or plastic deformation occurred.

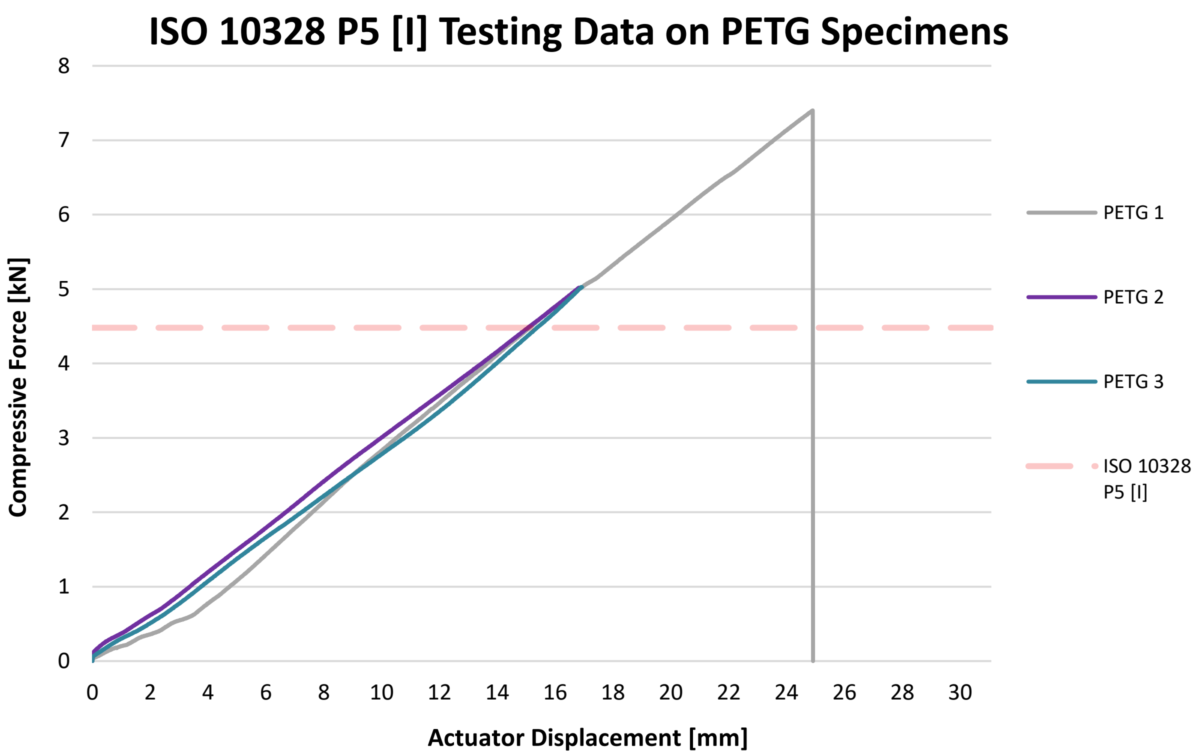

Figure 4.1: Results Graph of ISO 10328 P5 [I] Testing Data on PETG Specimens

4.2 Failure Mode

The failure of PETG 1 occurred due to a brittle fracture at the posterior distal end, which is consistent with similar studies (Marinopoulos et al., 2023). Figure 4.2a shows the top part of PETG 1 that broke off and separated from the bottom part, shown in Figure 4.2b, including the attachment plate. The PETG 1 fracture failure was sudden, with a linear load-displacement response up to failure and no indication of plastic deformation. Brittle behaviour of the PETG specimens was attributed to the printing temperature being at the higher end of the manufacturer's specified range. To increase ductility, various printing temperatures could be tested however, this may affect interlayer adhesion. Fracture occurred along the layer lines but also cracked across multiple layer lines, as shown in Figure 4.2c, indicating good interlayer adhesion resulting in more anisotropic behaviour. The attachment region at the distal end, which separated during testing, is shown in Figure 4.2d.

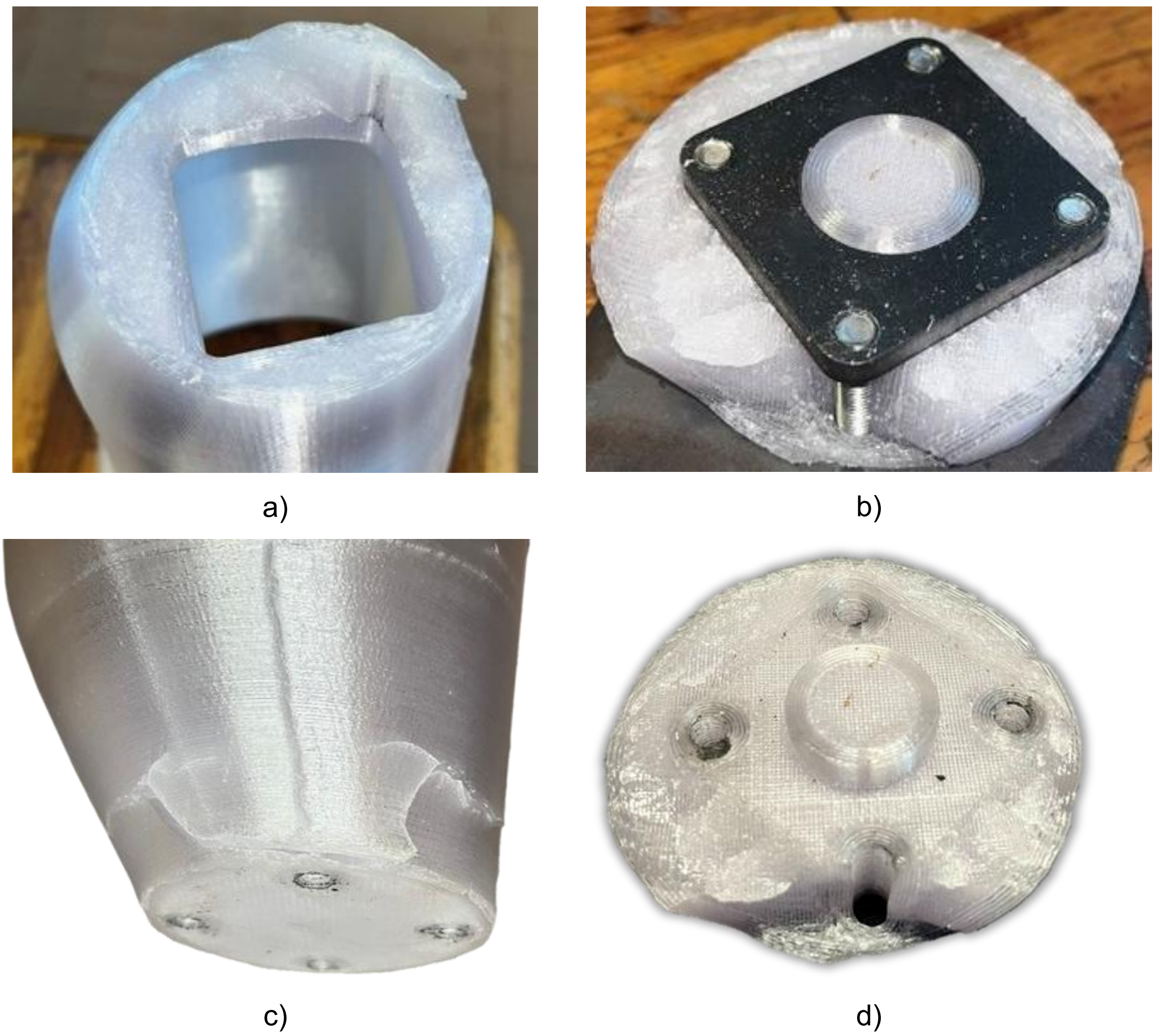

Figure 4.2: PETG 1 failure a) Top part; b) Bottom part; c) Fracture at the anterior distal end; d) Distal end failure interface.

The subsequent specimens, PETG 2 and PETG 3, were limited to 5 kN loading. Both specimens displayed no visible signs of damage at the posterior distal end, as shown on PETG 2 in Figure 4.3a, and PETG 3 in Figure 4.3b.

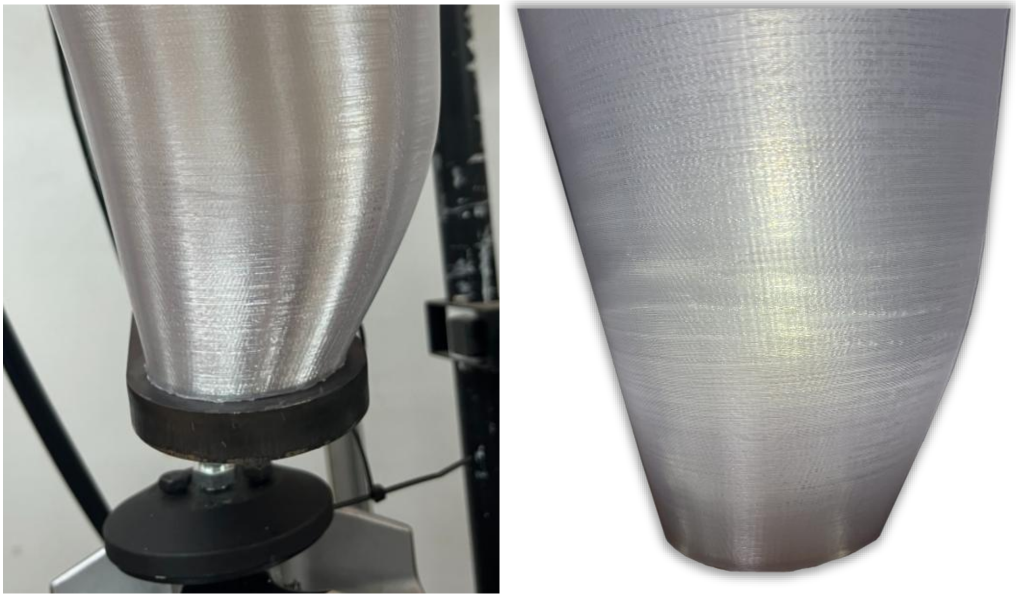

Figure 4.3: (a) PETG 2 distal end post-testing (b) PETG 3 distal end post-testing.

4.3 FEA Qualitative Comparison

The quantitative accuracy of the FEA predictions was limited due to the use of generic material data, linear static assumptions, and boundary condition simplifications, as discussed in Chapter 2.5.2 . However, the stress predictions still aligned qualitatively. In Figure 4.4a, the bottom part of PETG 1 is shown after failure. Although a crack is visible at the lower hole, this location does not represent the failure's origin. Instead, it reflects the final point of material separation as the fracture propagated, and the remaining section of the socket ultimately failed. The fracture propagated from the corner indicated by the arrow in Figure 4.4a, consistent with the location of stress hotspots predicted in the FEA simulations used for the comparative analysis between concept designs, shown in Figure 4.4b. The corner indicated in these figures is located at the posterior-lateral side of the socket.

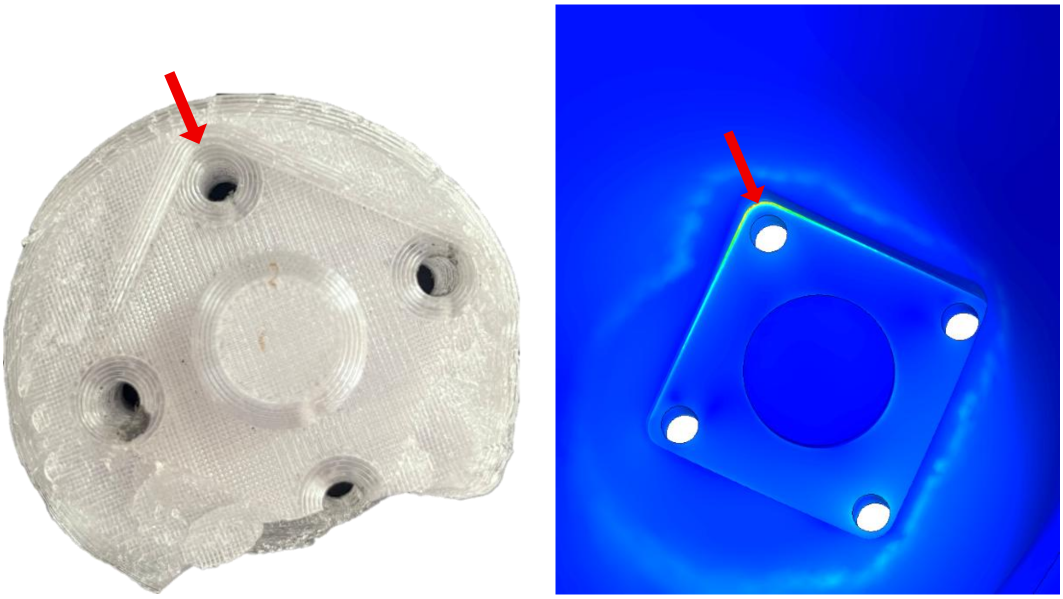

Figure 4.4: a) PETG 1 fracture location; b) FEA maximum von Mises stress location

The fracture in the outer wall of PETG 1 propagated horizontally in the direction of the layer lines, but also crossed layer lines as it progressed, as shown in Figure 4.5a. This was indicative of good layer adhesion. Compared to the FEA results, the fracture starting point is located at a similar height and location as the highest von Mises stress, as shown in Figure 4.5b.

Figure 4.5: a) PETG 1 fracture location external; b) FEA Highest von Mises Stress internal iso-clipping

4.4 Summary

The load-displacement results from physical testing were first presented. PETG 1 exhibited a brittle fracture and failed catastrophically at 7.2 kN. Since PETG 2 and PETG 3 had already exceeded the ISO 10328 P5 [I] requirement at that load, and additional failures could have damaged the rig, testing was halted at 5 kN. In analysing the failure mode, it was concluded that PETG 1 failed by brittle fracture, with crack propagation occurring both horizontally and across layer lines, indicating good interlayer adhesion. A strong qualitative correlation was observed between the physical fracture locations and the FEA predictions, with failure initiating from the same high-stress area.

CHAPTER 5: CONCLUSION AND RECOMMENDATIONS

5.1 Conclusion

The study aimed to design and manufacture a custom TF socket using FDM and test it to ensure compliance with regulatory standards. Ultimate static strength testing, in accordance with ISO 10328, was used as the standard for validating the final design and material selection. Concept designs for a TF socket were created from stump geometry obtained by 3D scanning an existing TF prosthetic socket. Two concept designs were developed utilising mesh editing software and SOLIDWORKS. The final design was selected through a comparative analysis using FEA simulation based on ISO 10328 loading conditions. Additionally, the worst-case loading conditions were obtained from FEA to be used for structural testing. Test specimens of the final design were manufactured using FDM. Three PETG sockets and two ePA-CF sockets were produced. As manufacturing the ePA-CF sockets presented several challenges, structural testing in accordance with ISO 10328 P5 [I] was commenced.

All PETG test specimens successfully met the ISO 10328 P5 [I] static strength requirement of withstanding 4.48 kN without failure. The first specimen failed catastrophically at 7.2 kN, causing damage to the testing rig. Subsequent tests were therefore limited to 5 kN to ensure compliance with the standard and prevent further damage. The failure resulted from a brittle fracture at the attachment plate. This failure location matched qualitatively with stress concentrations predicted in the FEA, confirming the validity of the simulated stress distribution, although the absolute stress predictions were limited by the assumptions of generic material data and linear static analysis. The load-displacement responses of the PETG sockets demonstrated high stiffness and a brittle fracture profile, with no observable plastic deformation, indicating that PETG can provide the required structural strength during static loading.

Beyond strength performance, PETG also proved beneficial in terms of practicality, cost, and availability. Furthermore, the clear PETG filament used in this study offered a unique clinical advantage in the potential to function as a check socket, enabling prosthetists to visually evaluate residual limb fit before progressing to definitive designs. However, it should be noted that PETG material properties, like most FDM materials, tend to vary between manufacturers, which highlights the need for careful material selection and quality control in clinical applications.

Manufacturing feasibility was also demonstrated with the printing of the PETG specimens, which produced near-flawless parts. The initial print time of 36 hours for a full socket was reduced to 28 hours through the optimisation of printing parameters, and further reductions are achievable with newer-generation FDM printers' improved speed. In contrast, the ePA-CF specimens presented significant manufacturing challenges, including bed-adhesion problems, warping, and nozzle deposition defects, which significantly undermined the print quality and structural integrity of the sockets, eliminating their viability for structural testing.

Overall, the results of this study suggest that PETG is currently a suitable material for additively manufactured TF prosthetic sockets using FDM. It met the requirements for the ultimate static strength test in accordance with ISO 10328 P5 loading condition [I]. Although the performance of the tested sockets was satisfactory, further tests are required by the standard to confirm full compliance.

5.2 Recommendations for future work

Future work should expand the investigation of additive-manufactured prosthetic sockets by exploring several key areas:

Firstly, moving beyond ultimate static strength testing to include cyclic testing as prescribed by ISO 10328. Future designs could consider integrating common suspension systems, such as pin-lock, suction, or vacuum mechanisms, to evaluate the effects of cut-outs, ports, and hardware interfaces on structural performance under standardised loading as well.

There would also be substantial value in exploring additional FDM materials, particularly as the range of available polymers continues to grow. Simultaneously investigating the influence of printing parameters on material performance through comprehensive experimental testing would also generate reliable material data. Extensive material data would enhance the use of FEA for design refinement, especially through techniques such as topology optimisation and strategic thickness mapping, which could reduce mass while ensuring that the socket maintains sufficient strength in accordance with ISO 10328 requirements.

Lastly, testing can be extended to a broader range of patient-specific geometries—including variations in residual limb length, circumference, and soft-tissue composition—to better understand how these factors influence the structural performance of the socket.

REFERENCES

Abdulrahman, S.A., Hamad, Q.A. & Oleiwi, J.K. 2021. Investigation of some properties for laminated composite used for prosthetic socket. *Engineering and Technology Journal*. *University of Technology-Iraq*. 39(11):1625–1631.

Al-Masa'fah, W., Abushaikha, I. & Bwaliez, O.M. 2025. Exploring the role of additive manufacturing in the prosthetic supply chain: qualitative evidence. *The TQM Journal*. *Emerald Publishing Limited*. 37(7):1963–1991.

Borthakur, P.P. 2025. The role and future directions of 3D printing in custom prosthetic design. *Engineering Proceedings*. *MDPI*. 81(1):10.

Chen, R.K., Jin, Y., Wensman, J. & Shih, A. 2016. Additive manufacturing of custom orthoses and prostheses—A review. *Additive Manufacturing*. 12:77–89.

Ebrahim, M.A.-B. 2015. 3D laser scanners' techniques overview. *Int J Sci Res*. 4(10):323–331.

Engstrom, B. & Van de Ven, C. 1999. Therapy for amputees. 3rd ed. Elsevier Health Sciences.

Fergason, J. & Smith, D.G. 1999. Socket considerations for the patient with a transtibial amputation. *Clinical Orthopaedics and Related Research*. *LWW*. 361:76–84.

Gariboldi, F., Pasquarelli, D. & Cutti, A.G. 2022. Structural testing of lower-limb prosthetic sockets: a systematic review. *Medical engineering & physics*. *Elsevier*. 99:103742.

Gerschutz, M.J., Haynes, M.L., Nixon, D.M. & Colvin, J.M. 2011. Tensile strength and impact resistance properties of materials used in prosthetic check sockets, copolymer sockets, and definitive laminated sockets. *Journal of Rehabilitation Research & Development*. 48(8):987–1004.

Gholizadeh, H., Osman, N.A.A., Eshraghi, A. & Ali, S. 2014. Transfemoral prosthesis suspension systems: a systematic review of the literature. *American journal of physical medicine & rehabilitation*. *LWW*. 93(9):809–823.

Graebner, R.H. & Current, T.A. 2007. Relative strength of pylon-to-socket attachment systems used in transtibial composite sockets. *JPO: Journal of Prosthetics and Orthotics*. *LWW*. 19(3):67–74.

Haghsefat, K. & Tingting, L. 2020. FDM 3D Printing Technology and Its Fundemental Properties.

Haleem, A. & Javaid, M. 2019. 3D scanning applications in medical field: a literature-based review. *Clinical Epidemiology and Global Health*. *Elsevier*. 7(2):199–210.

Hsueh, M.H., Lai, C.J., Wang, S.H., Zeng, Y.-S., Hsieh, C.-H., Pan, C.-Y. & Huang, W.-C. 2021. Effect of printing parameters on the thermal and mechanical properties of 3d-printed PLA and PETG, using fused deposition modeling. *Polymers*. *MDPI*. 13(11):1758.

Huysamen, H.W., Kinnear, W.A., Fonternel, T.E., Turton, E., Yadroitsava, I. & Yadroitsev, I. 2020. 3D printed laryngoscope for endotracheal intubation. *South African Journal of Industrial Engineering*. *The Southern African Institute for Industrial Engineering*. 31(3):209–217.

Isa, A., Nosbi, N., Che Ismail, M., Md Akil, H., Wan Ali, W.F.F. & Omar, M.F. 2022. A review on recycling of carbon fibres: Methods to reinforce and expected fibre composite degradations. *Materials*. *MDPI*. 15(14):4991.

ISO10328. 2016. ISO 10328:2016 Prosthetics: Structural testing of lower-limb prostheses - Requirements and test methods. *International Organisation for Standardisation*.

ISO52900. 2021. ISO 52900:2021Additive manufacturing — General principles — Fundamentals and vocabulary. *International Organisation for Standardisation*.

Jia, X., Zhang, M. & Lee, W.C.C. 2004. Load transfer mechanics between trans-tibial prosthetic socket and residual limb-dynamic effects. *J Biomech*. 37(9):1371–7.

Johannesson, A., Larsson, G.-U., Ramstrand, N., Lauge-Pedersen, H., Wagner, P. & Atroshi, I. 2010. Outcomes of a standardized surgical and rehabilitation program in transtibial amputation for peripheral vascular disease: a prospective cohort study. *American journal of physical medicine & rehabilitation*. *LWW*. 89(4):293–303.

Jones, R., Haufe, P., Sells, E., Iravani, P., Olliver, V., Palmer, C. & Bowyer, A. 2011. RepRap-the replicating rapid prototyper. *Robotica*. *Cambridge University Press*. 29(1):177–191.

Kamrad, I., Söderberg, B., Örneholm, H. & Hagberg, K. 2020. SwedeAmp—the Swedish Amputation and Prosthetics Registry: 8-year data on 5762 patients with lower limb amputation show sex differences in amputation level and in patient-reported outcome. *Acta Orthopaedica*. 91(4):464–470.

Kim, S., Yalla, S.V., Shetty, S. & Rosenblatt, N.J. 2024. Structural integrity of custom-designed additive manufactured prosthetic sockets compared to traditional sockets. *Results in Materials*. *Elsevier*. 21:100549.

Krouskop, T., Muilenberg, A. & Doughtery, D. 1987. Computer-aided design of a prosthetic socket. *Journal of Rehabilitation Research & Development*. *Veterans Administration, Department of Medicine and Surgery, Rehabilitation*. 24(2):31–38.

Lenka, P.K., Choudhury, A.R. & others. 2011. Analysis of trans tibial prosthetic socket materials using finite element method. *Journal of Biomedical Science and Engineering*. *Scientific Research Publishing*. 4(12):762.

Marable, W.R., Smith, C., Sigurjónsson, B.Þ., Atlason, I.F. & Johannesson, G.A. 2020. Transfemoral socket fabrication method using direct casting: Outcomes regarding patient satisfaction with device and services. *Canadian Prosthetics & Orthotics Journal*. *Canadian Online Publication Group*. 3(2).

Marinopoulos, T., Li, S. & Silberschmidt, V.V. 2023. Structural integrity of 3D-printed prosthetic sockets: Experimental study for paediatric applications. *Journal of materials research and technology*. *Elsevier*. 24:2734–2742.

Miller, T.A., Paul, R., Forthofer, M. & Wurdeman, S.R. 2020. Impact of time to receipt of prosthesis on total healthcare costs 12 months postamputation. *American journal of physical medicine & rehabilitation*. *LWW*. 99(11):1026–1031.

Modular Assembly Technology South Africa. 2024. *LEVELING SWIVEL FOOT (5.22.100.16.130)*. https://moduasm.co.za/product/leveling-swivel-foot-5-22-100-16-130/ Date of access: 24 Sep. 2024

Myers, M. & Chauvin, B.J. 2021. Above the knee amputations. StatPearls Publishing.

Nguyen, D.P., San Tran, T., Tran, H.Y., Nguyen, N.P., Vo, T.M., Pham, T.H.N., Nguyen, V.T., Nguyen, T.T. & others. 2025. Effect of Materials on the Mechanical Properties of Fused Deposition Modeling Three-Dimensional Printed Products. *Journal of Technical Education Science*. 20(01):1–11.

Normann, E., Olsson, A. & Brodtkorb, T.-H. 2011. Modular socket system versus traditionally laminated socket: a cost analysis. *Prosthetics and orthotics international*. *SAGE Publications UK*. 35(1):76–80.

Oldfrey, B., Miodownik, M., Barbareschi, G., Williams, R. & Holloway, C. 2020. Digital Fabrication of Lower Limb Prosthetic Sockets. *AT2030*.

Owen, M.K. & DesJardins, J.D. 2020. Transtibial prosthetic socket strength: the use of ISO 10328 in the comparison of standard and 3D-printed sockets. *JPO: Journal of Prosthetics and Orthotics*. *LWW*. 32(2):93–100.

Paternò, L., Ibrahimi, M., Gruppioni, E., Menciassi, A. & Ricotti, L. 2018. Sockets for limb prostheses: a review of existing technologies and open challenges. *IEEE Transactions on Biomedical Engineering*. *IEEE*. 65(9):1996–2010.

Paul, S. 2021. Finite element analysis in fused deposition modeling research: A literature review. *Measurement*. *Elsevier*. 178:109320.

Physiopedia. 2022. *Lower Limb Prosthetic Sockets and Suspension Systems*. https://www.physio-pedia.com/index.php?title=Lower_Limb_Prosthetic_Sockets_and_Suspension_Systems&oldid=295136 Date of access: 21 Mar. 2022

Pousett, B., Lizcano, A. & Raschke, S.U. 2019. An investigation of the structural strength of transtibial sockets fabricated using conventional methods and rapid prototyping techniques. *Canadian Prosthetics & Orthotics Journal*. 2(1).

Pribanić, T., Petković, T., Donlić, M., Angladon, V. & Gasparini, S. 2016. 3D structured light scanner on the smartphone., in: Image Analysis and Recognition: 13th International Conference, ICIAR 2016, in Memory of Mohamed Kamel, Póvoa de Varzim, Portugal, July 13-15, 2016, Proceedings 13. pp. 443–450.

Radcliffe M.S, C.W. 1955. Functional considerations in the fitting of above-knee prostheses. *Artificial Limbs*. 2(1):35–60.

Ricaurte, E.M., Mahmoud, N. & others. 2018. Medical Certification Strategies in Response to Technologically Advanced Prosthetic Devices.

Skoglund, P. 2015. Prosthetic socket in Titanium: An outer shell prosthetic socket for a lower-leg amputee manufactured in Ti6Al4V by Electron Beam Melting.

Tekinalp, H.L., Kunc, V., Velez-Garcia, G.M., Duty, C.E., Love, L.J., Naskar, A.K., Blue, C.A. & Ozcan, S. 2014. Highly oriented carbon fiber-polymer composites via additive manufacturing. *Composites Science and Technology*. *Elsevier*. 105:144–150.

Vogt, M., Rips, A. & Emmelmann, C. 2021. Comparison of iPad Pro's LiDAR and TrueDepth capabilities with an industrial 3D scanning solution. *Technologies*. *MDPI*. 9(2):25.

Waihanga, P. 2022. *Suspension Systems - Peke Waihanga Artificial Limb Service*. https://www.pw.co.nz/products/categories/suspension-systems Date of access: 31 Mar. 2022

Wong, K.V. & Hernandez, A. 2012. A review of additive manufacturing. *International scholarly research notices*. *Hindawi*. 2012.

APPENDIX A: LINEAR STATIC FEA RESULTS

The structural response of both socket designs under identical loading conditions was compared using FEA. A linear static analysis was carried out, acknowledging the limitations related to the anisotropic and nonlinear behaviour of FDM materials, as was covered in Chapter 3.5. As a result, rather than emphasising absolute accuracy, the FEA results are used for comparison between designs.

A-1 Socket Design 1

The FEA simulations aimed to evaluate the initial geometry of Socket Design 1 and extract the maximum von Mises stress. The results are presented and discussed in terms of von Mises stress.

A-1.1 P5 [I]

The location of the maximum von Mises stress for loading condition P5 [I] is indicated in Figure A.1. As seen on the plot, this is located on the anterior medial side of the socket in the hole of the fastener.

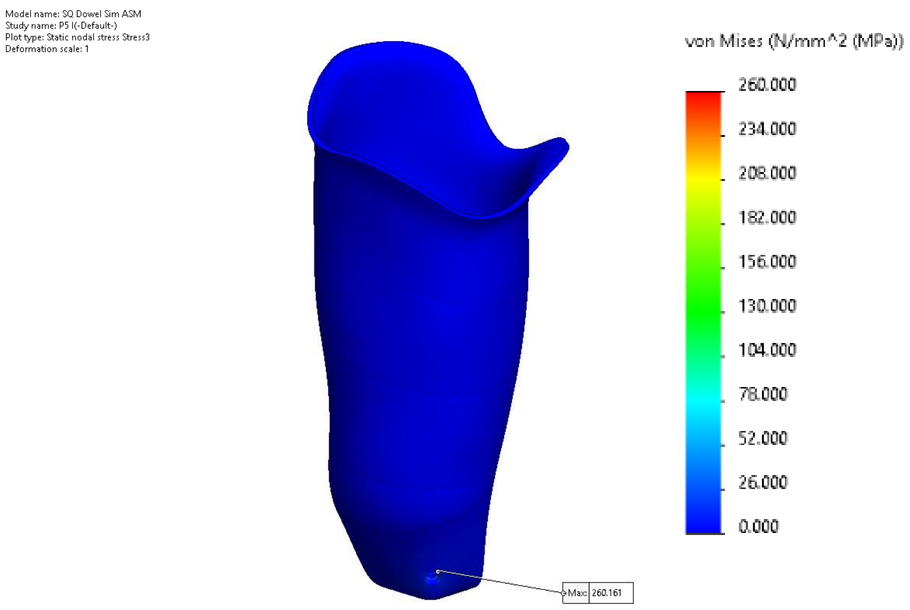

Figure A.1: Maximum von Mises stress location of Socket Design 1 P5 [I]

The stresses developed in the fastener hole of the socket are due to the contact forces developing on the edges of the fastener-socket interface, as shown in Figure A.2.

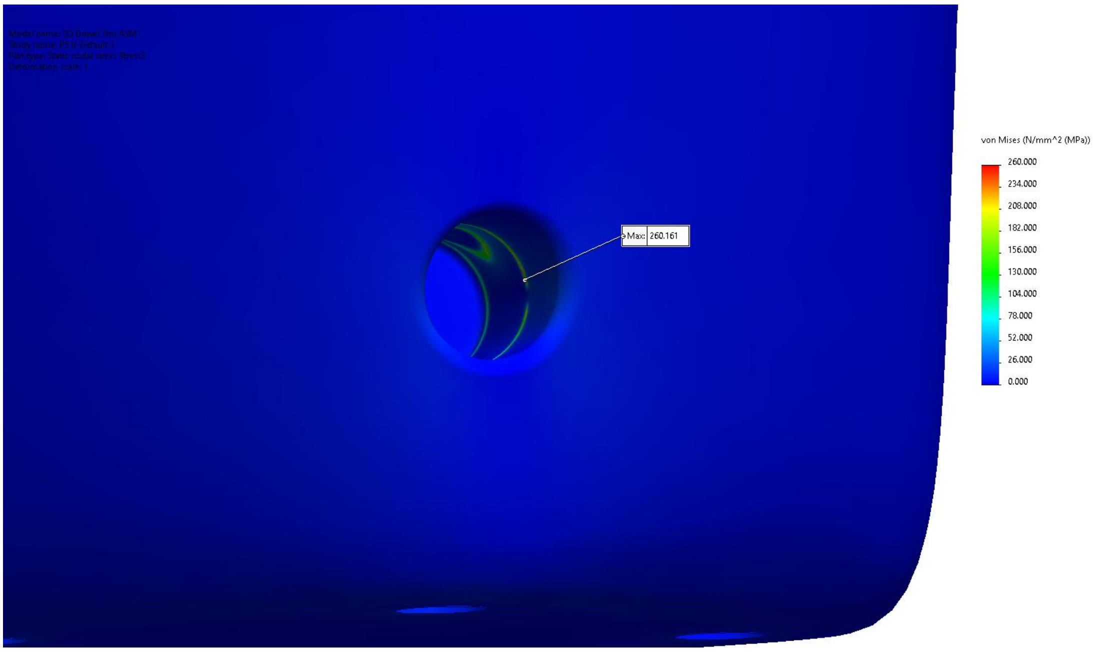

Figure A.2: Von Mises stress at the fastener-socket interface

Figure A.3 shows an enlarged view of the exact node at which the maximum von Mises stress occurs. The mesh is also displayed on the plot. The mesh on the fastener, as well as the contact face on the socket was refined to 0.5 mm element size to ensure convergence of the results as far as possible while remaining computationally viable for the available hardware.

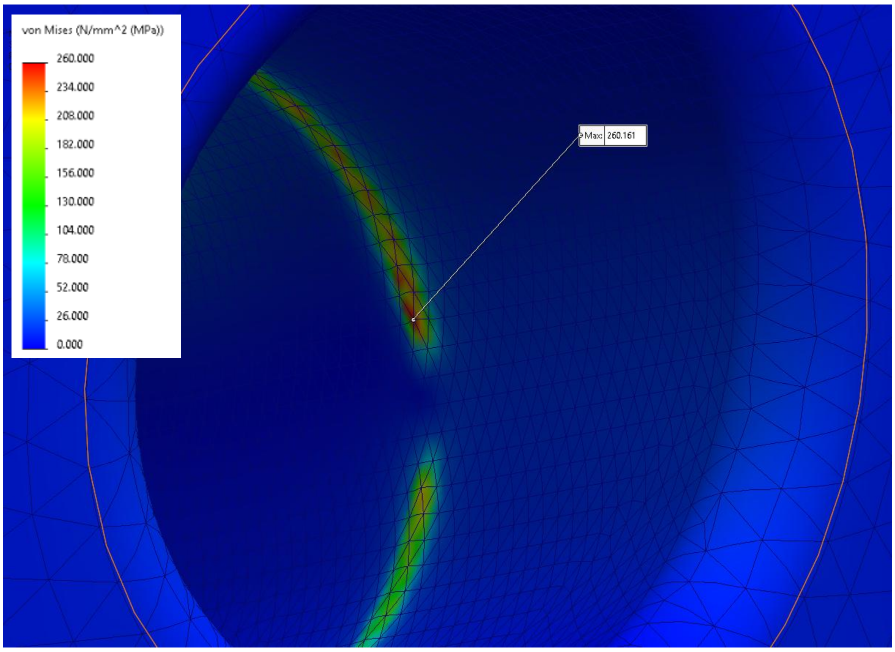

Figure A.3: Enlarged region of maximum von Mises stress of Socket Design 1 P5 [I]

A-1.2 P5 [II]

The location of the maximum von Mises stress for loading condition P5 [II] is indicated in Figure A.4. Similar to loading condition P5 [I], the maximum stress is located at the anterior medial side of the socket in the hole of the fastener.

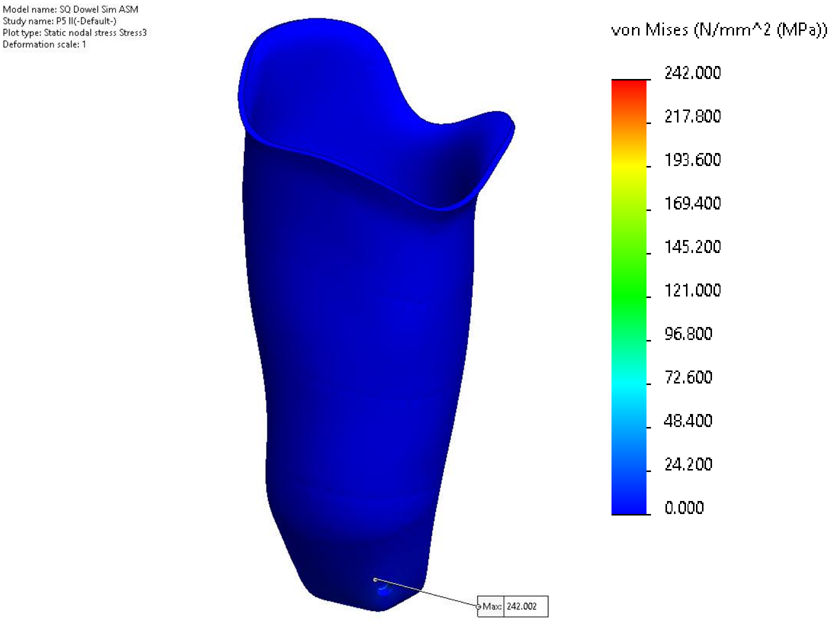

Figure A.4: Maximum von Mises stress location of Socket Design 1 P5 [II]

The stress concentrations shown in Figure A.5, developed on the edges of the fastener-socket interface, similar to loading condition P5 [I]. The enlarged view shows the exact node at which the maximum von Mises stress occurs, on the opposite side of the hole than the previous loading condition. The magnitude of the maximum von Mises stress was slightly lower in loading condition II. The mesh is also displayed on the plot and was kept similar for both load cases.

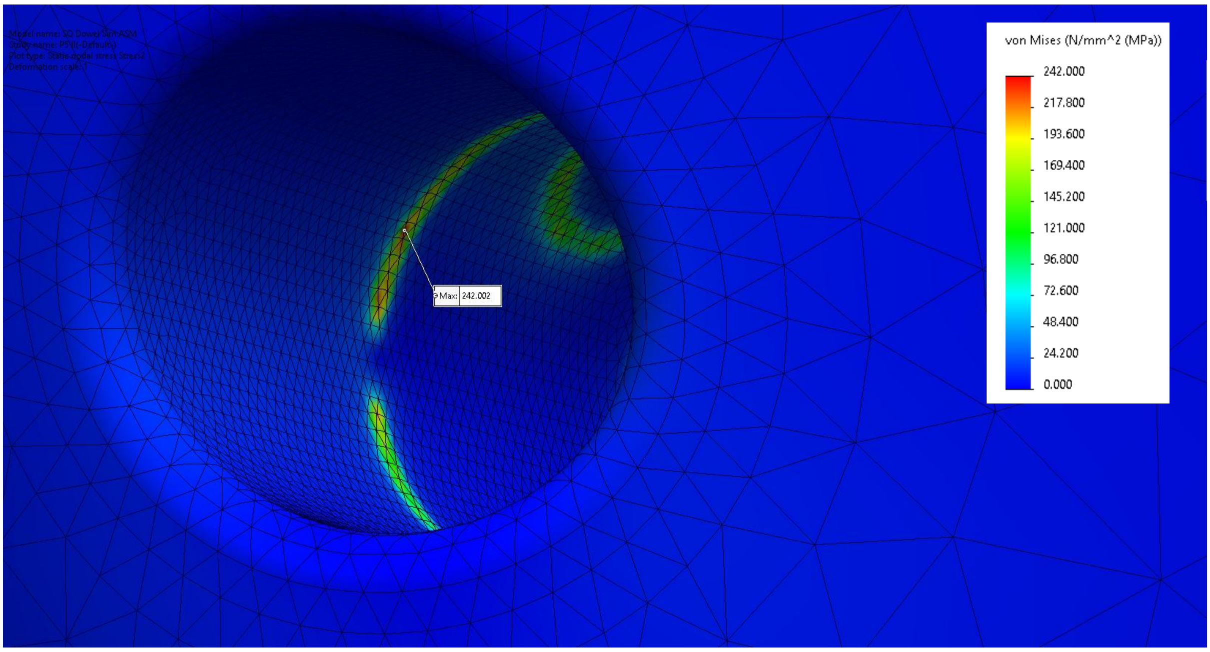

Figure A.5: Enlarged region of the maximum von Mises stress of Socket Design 1 P5 [I]

A-2 Socket Design 2

The FEA simulations on Socket Design 2 are aimed at evaluating the maximum von Mises stress to be compared with the results of Socket Design 1. Identical boundary conditions and load cases were applied to ensure consistent comparison.

A-2.1 P5 [I]

The location of the maximum von Mises stress for loading condition P5 [I] is indicated in Figure A.6. In contrast with Socket Design 1, the maximum stress is located at the posterior lateral side of the socket in the corner of the attachment plate.

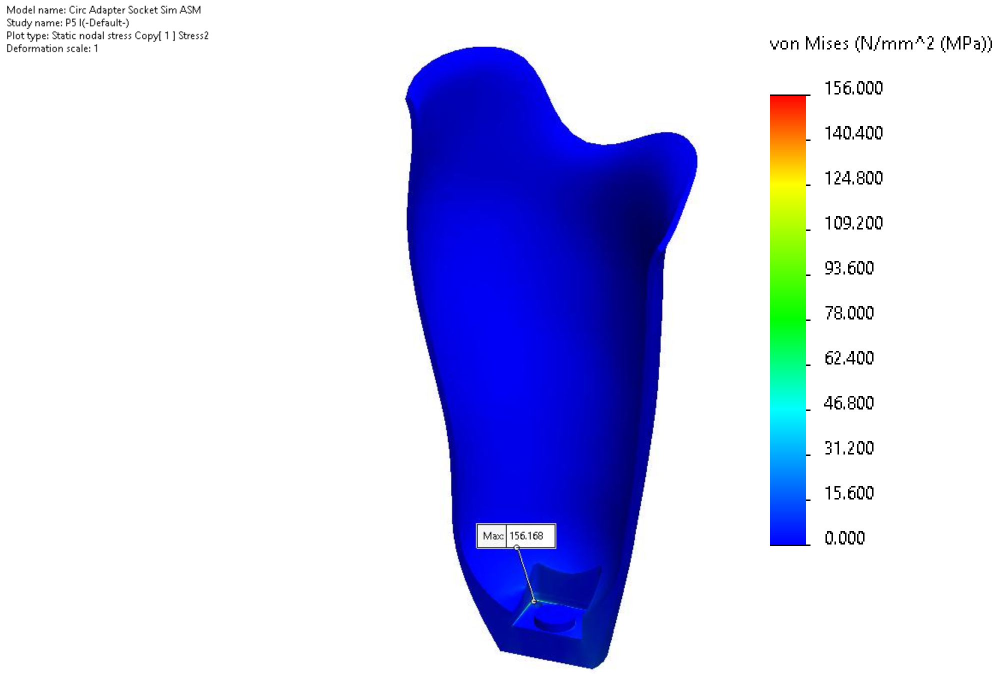

Figure A.6: Maximum von Mises stress location of Socket Design 2 P5 [I]

The stresses developed in the corner of the attachment plate cutout in the socket were due to the contact forces developing on the edges of the attachment plate-socket interface, as shown in Figure A.7.

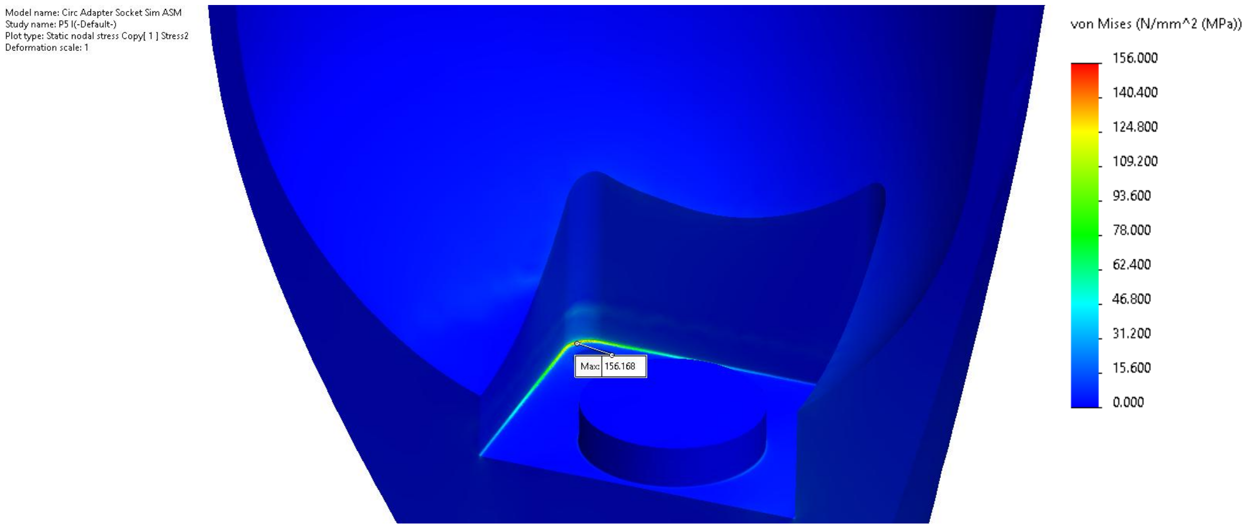

Figure A.7: Von Mises stress on the attachment plate-socket interface

Figure A.8 shows an enlarged view of the exact node at which the maximum von Mises stress occurs. The mesh is also displayed on the plot. The mesh on the attachment plate as well as the contact face on the socket was refined to 0.2mm element size to ensure convergence of the results as far as possible while remaining computationally viable for the available hardware.

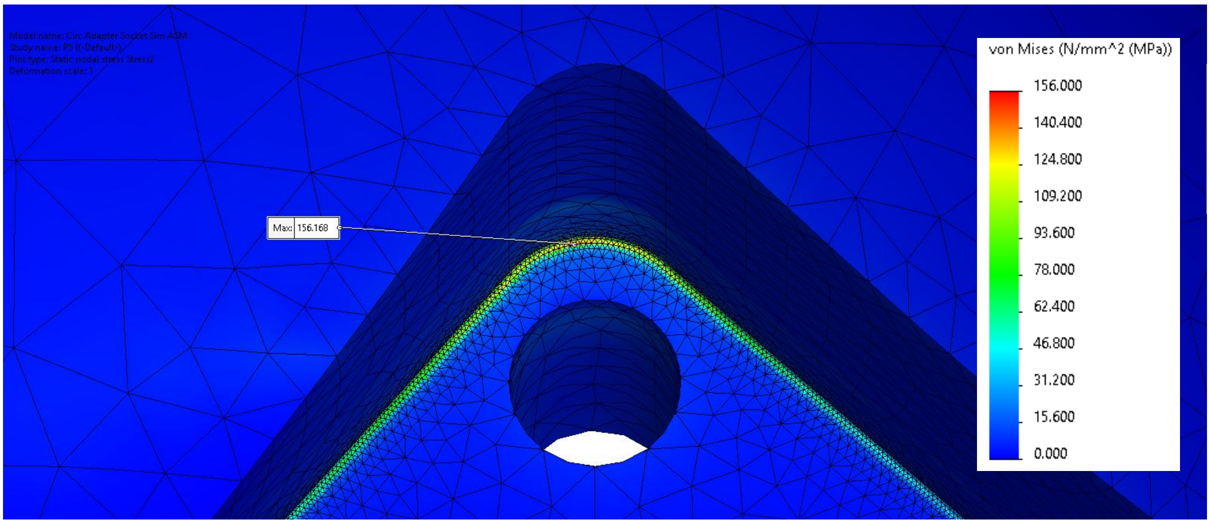

Figure A.8: Enlarged region of Maximum von Mises Stress of Socket Design 2 P5 I

A-2.2 P5 [II]

The location of the maximum von Mises stress for loading condition P5 II is indicated in Figure A.9. The location of the maximum stress is similar to loading condition P5 [I].

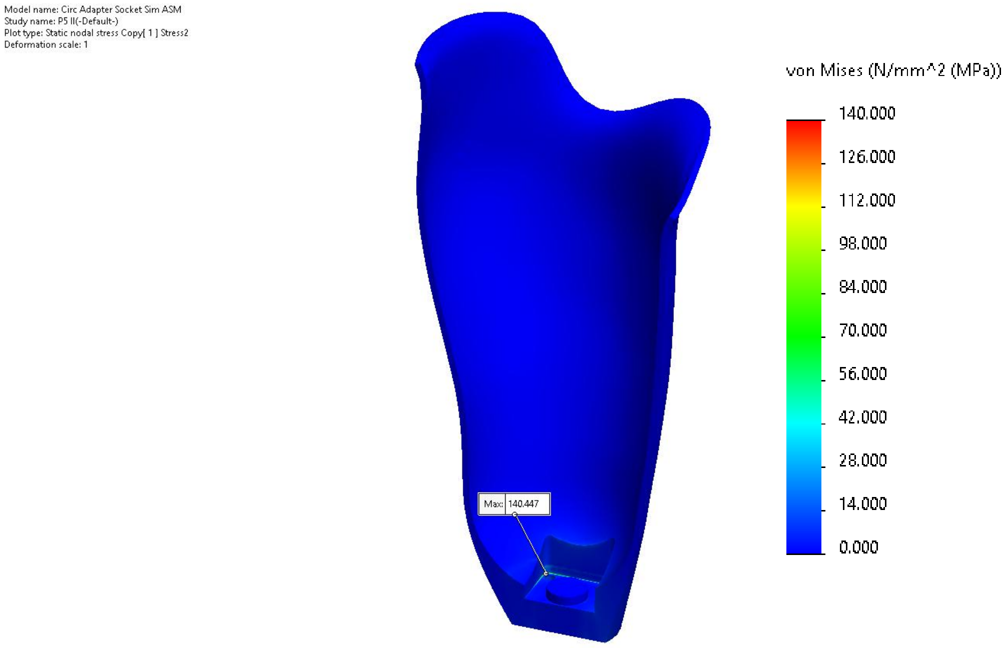

Figure A.9: Maximum von Mises stress location of Socket Design 2 P5 [II]

Figure A.10 shows an enlarged view of the exact node at which the maximum von Mises stress occurs, similar to loading condition P5 I. The magnitude of the maximum von Mises stress was slightly lower in loading condition [II]. The mesh is also displayed on the plot and was kept similar for both load cases.

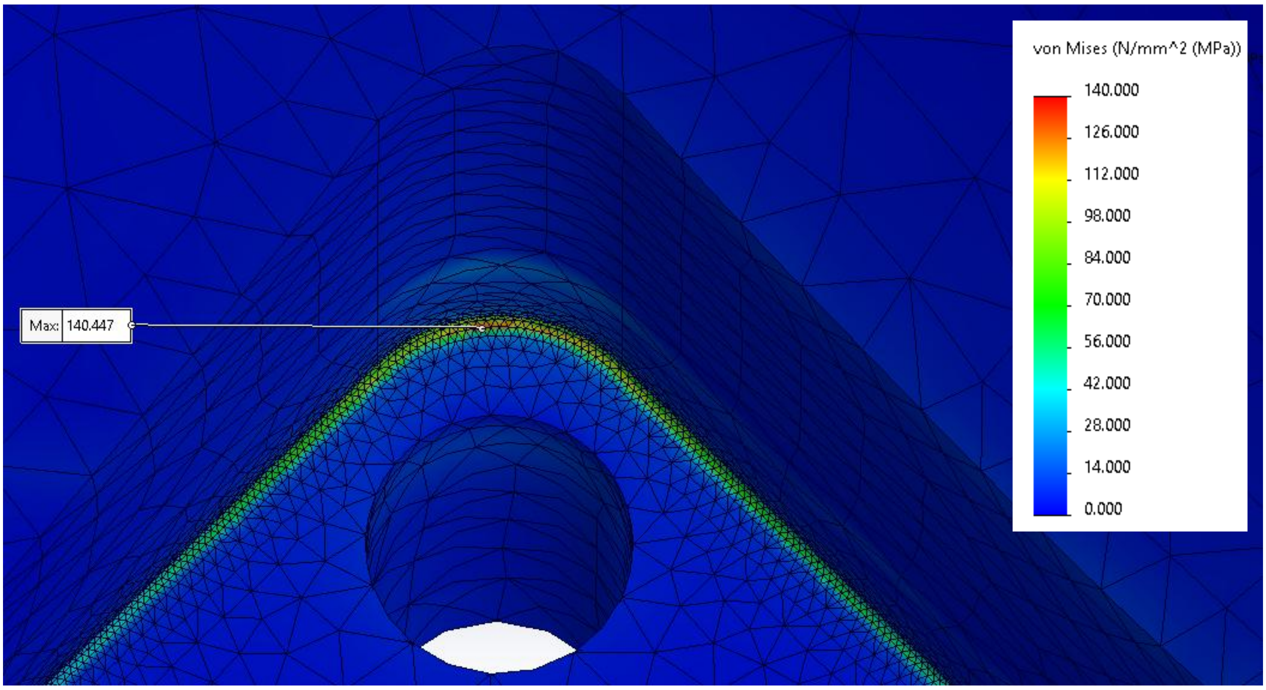

Figure A.10: Enlarged region of Maximum von Mises Stress of Socket Design 2 P5 [II]

APPENDIX B: TESTING RIG MANUFACTURING

For manufacturing the physical model of the stump, Smooth-Cast 300 White Urethane Plastic was used. The mould for casting the stump was 3D printed using a special setting in the slicer software called "Vase Mode". This produced a thin-walled mould, printed as a single line width, Figure B.11.

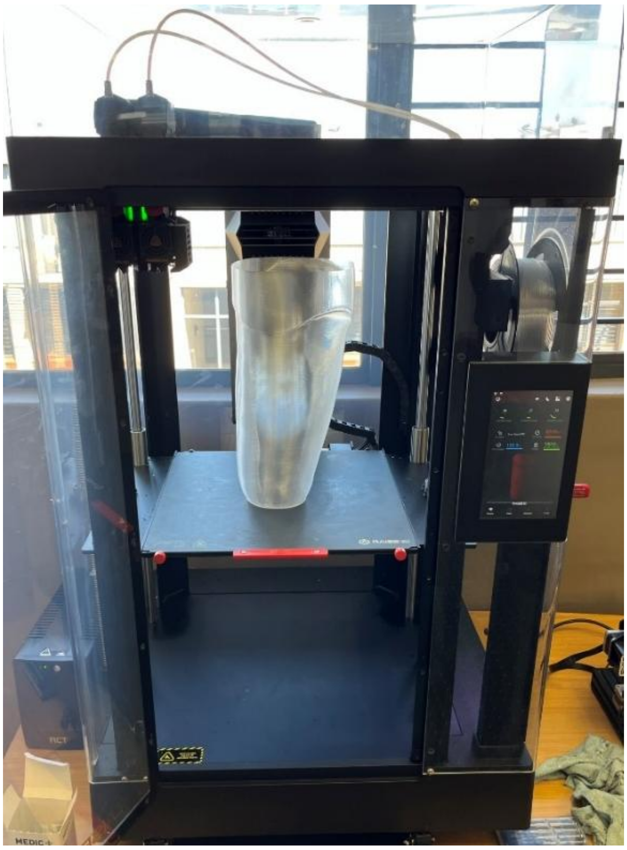

Figure B.11: 3D printed stump mould.

A steel pipe represents the femur for transferring applied loads to the stump during testing. The placement of the pipe had to be aligned with the distal end attachment as shown in Figure B.12.

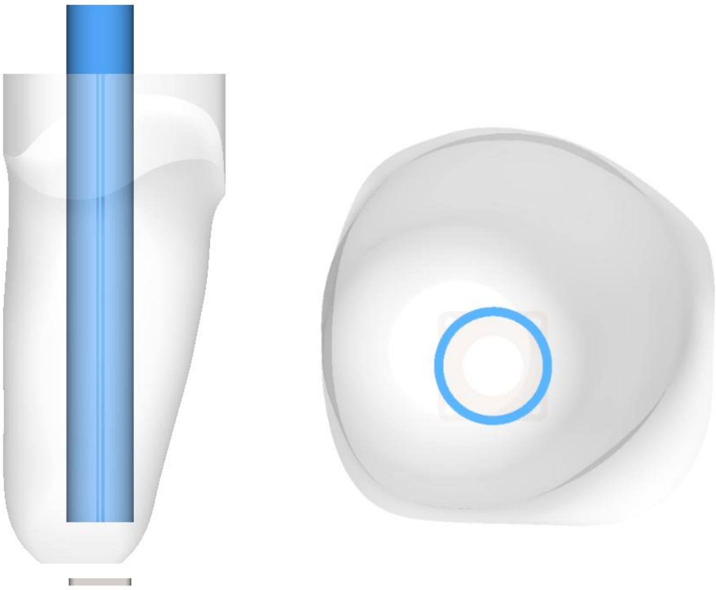

Figure B.12: Front and top view of the steel pipe stump alignment.

For the physical testing, a steel pipe with an outer diameter of 48.5mm and inner diameter of 41mm was press-fitted into the cut hole in the top plate and welded along the seams as shown in Figure B.13.

Figure B.13: Steel pipe welded to the top plate

To ensure accurate alignment of the physical model to the CAD model an alignment jig was 3D printed to assist with the alignment (Figure B.14). The alignment jig fitted on the stump mould and aligned the steel pipe with the exact location of the femur as designed in the CAD model. It also assisted in aligning the top plate correctly, which ensured accurate geometry for applying forces according to the ISO10328 calculations.

Figure B.14: Stump and Steel Pipe Alignment Jig

To clamp the test jig in a Universal Testing Machine (UTM) and accurately apply the fixtures and loads, a ball-joint type connection was needed. A suitable solution was M16 levelling swivel feet, shown in Figure B.15, which is rated at 10kN static load with a sufficient angle range of 30°.

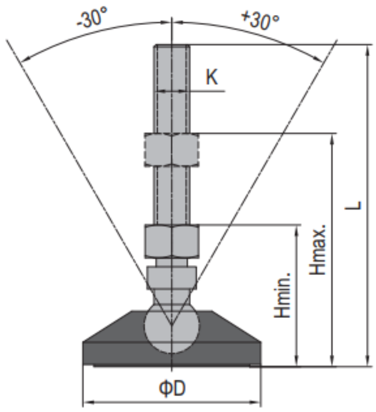

D (mm)	KxL (mm)	H min. (mm)	H max. (mm)	Max. Static Load 最大静态载荷 (N)
99	M16x130	45	100	10000

Figure B.15: M16 Levelling Swivel Foot (Image source: (Modular Assembly Technology South Africa, 2024))

Some modifications had to be made to ensure compatibility with the UTM's clamps. Two 6mm holes were drilled in the foot for inserting M6 bolts, which could be clamped by the UTM. The purpose of the bolts was only to hold the testing jig in place, as the compressive force of the machine was still being applied by the clamps to the levelling swivel foot, shown in Figure B.16.

Figure B.16: Clamping condition of the levelling swivel foot

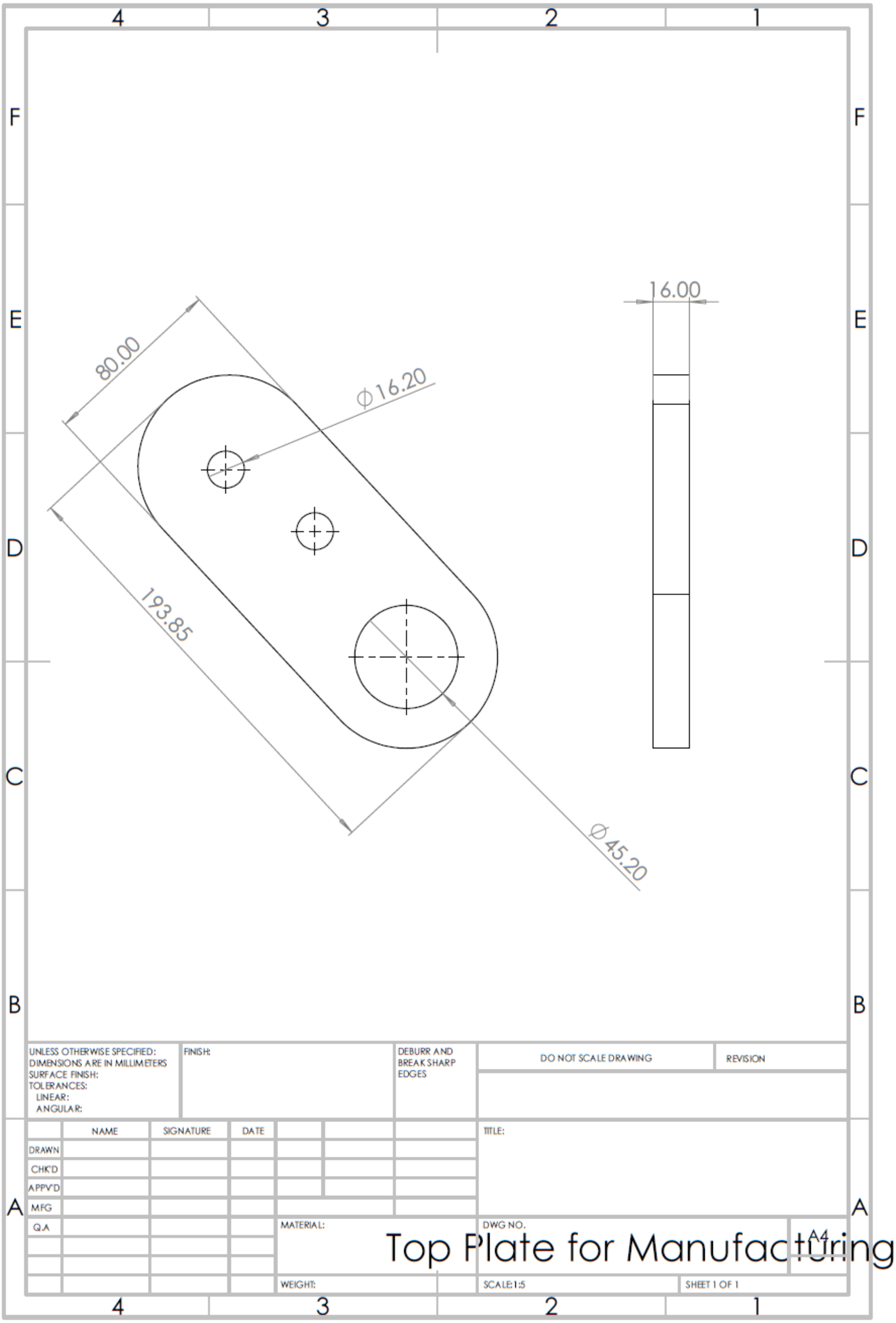

Figure B.17: Initial Top Plate Manufacturing Drawing

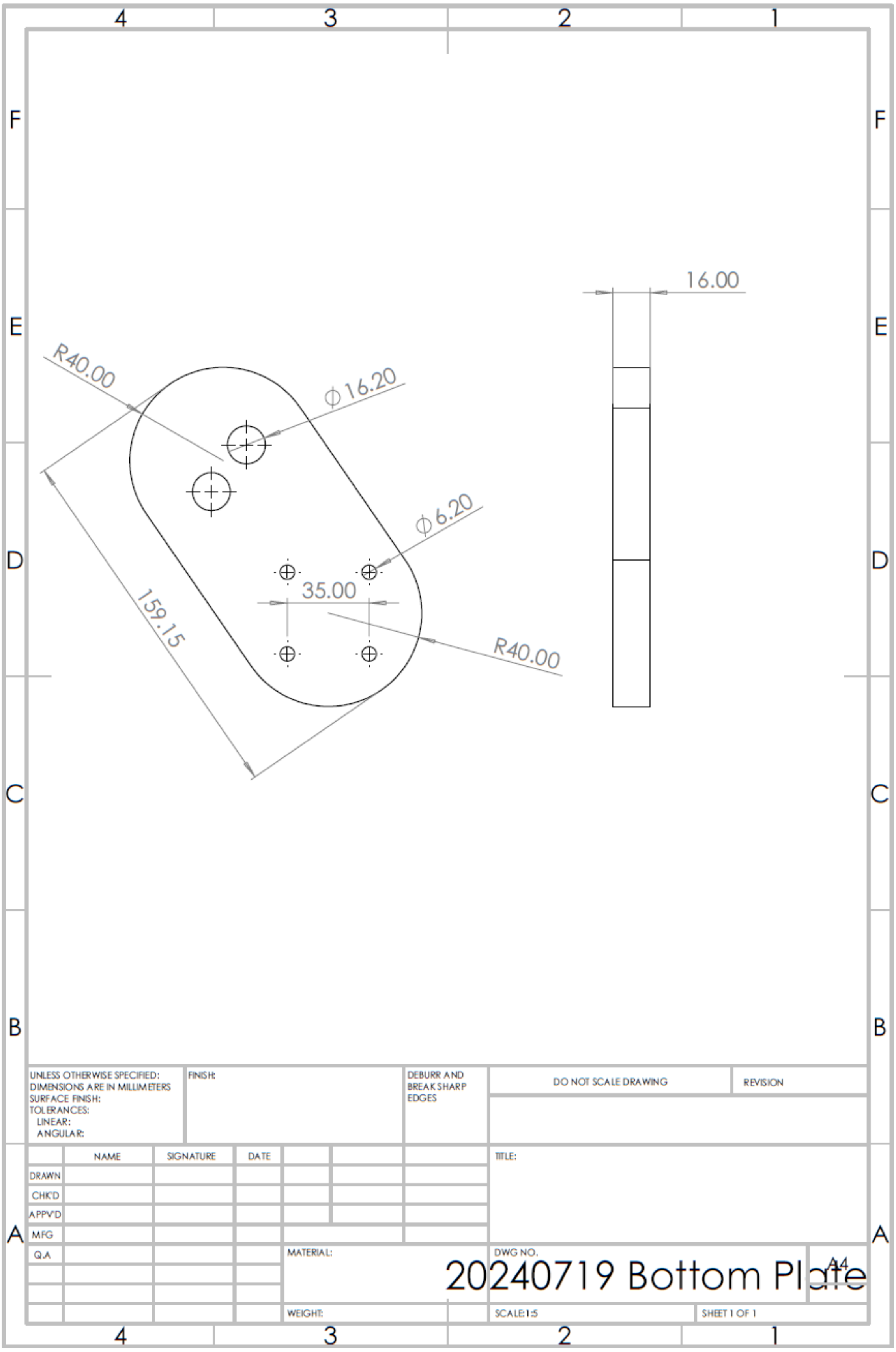

Figure B.18: Bottom Plate Manufacturing Drawings

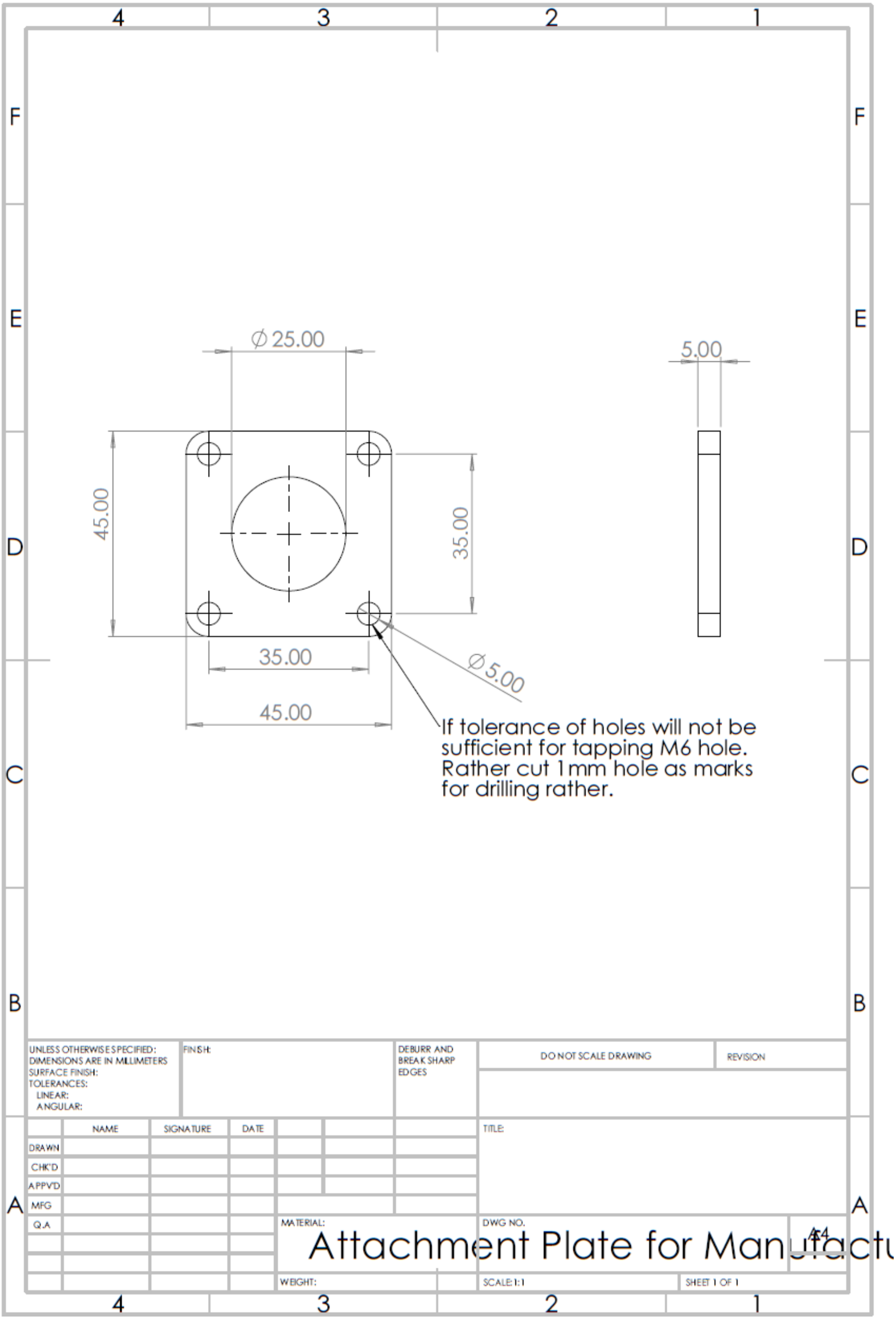

Figure B.19: Attachment Plate Manufacturing Drawings

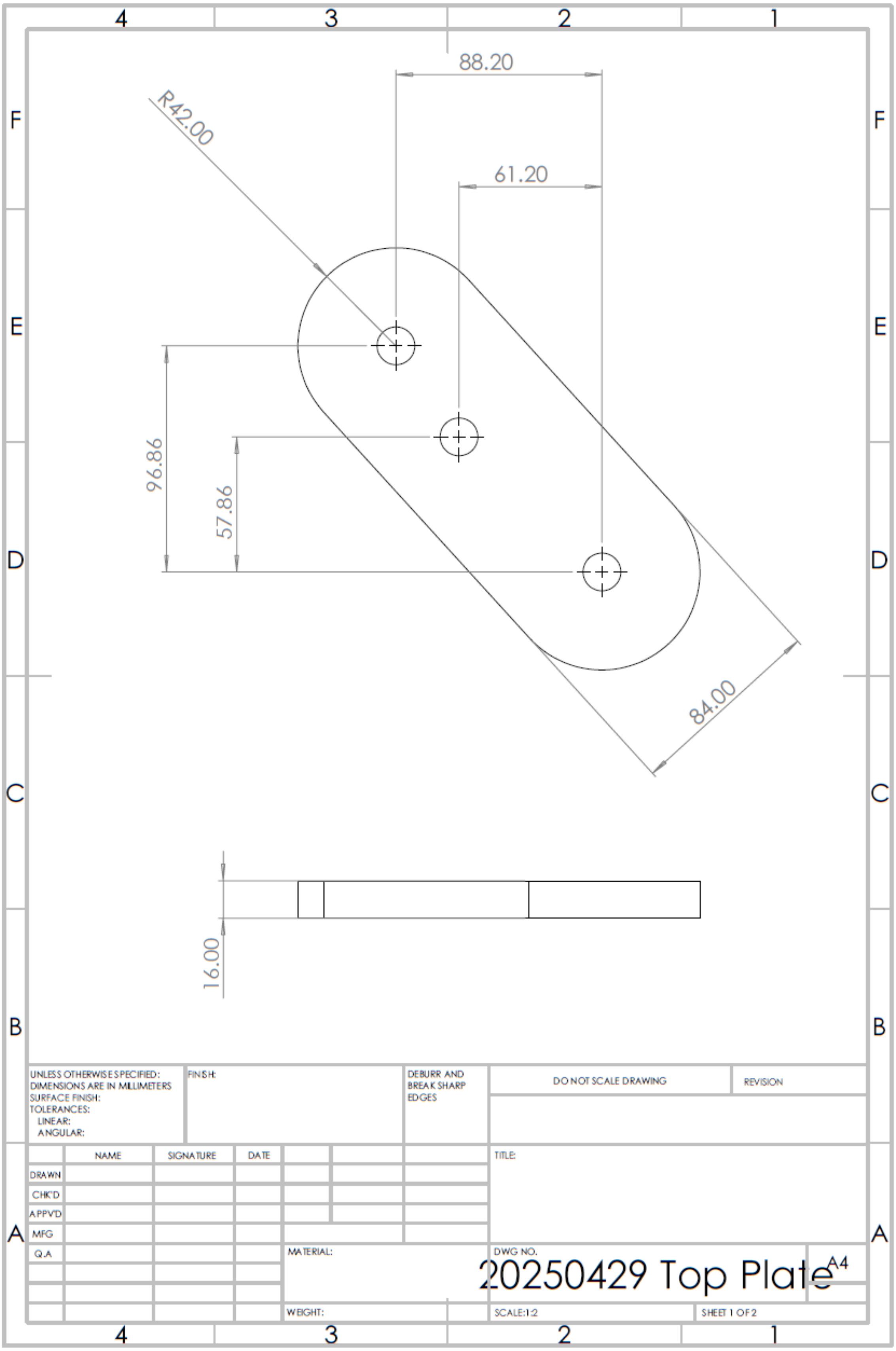

Figure B.20: Rectified Top Plate Manufacturing Drawings

APPENDIX C: ISO 10328 REVISED CALCULATIONS

Table C.1: Revised reference dimensions for loading forces, directions, and locations

Reference Plane	Offset Location	Dimensions for Test Loading Level P5 I [mm]
Knee	f_K	52
	o_K	-50
	u_K	500
Ankle	f_A	-32
	o_A	30
	u_A	80
New Top Plate	u_X2	956
	f_X2	143.20
	o_X2	-136.86

APPENDIX D: SOCKET MANUFACTURING

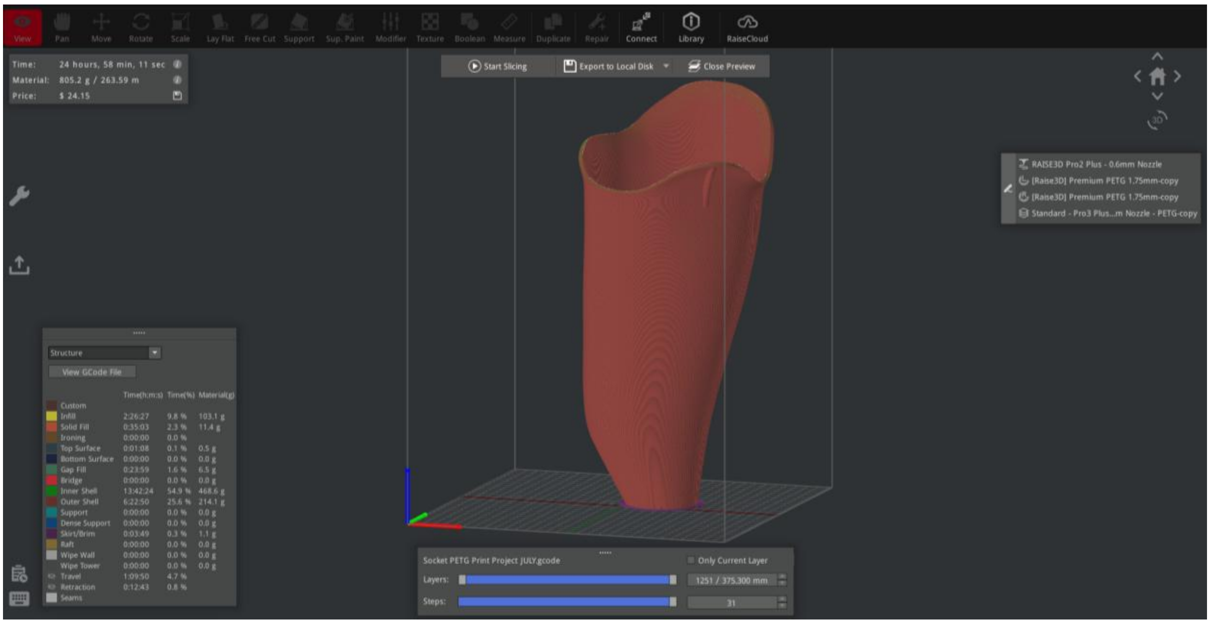

Figure D.21: Slicer information showing printing time and weight

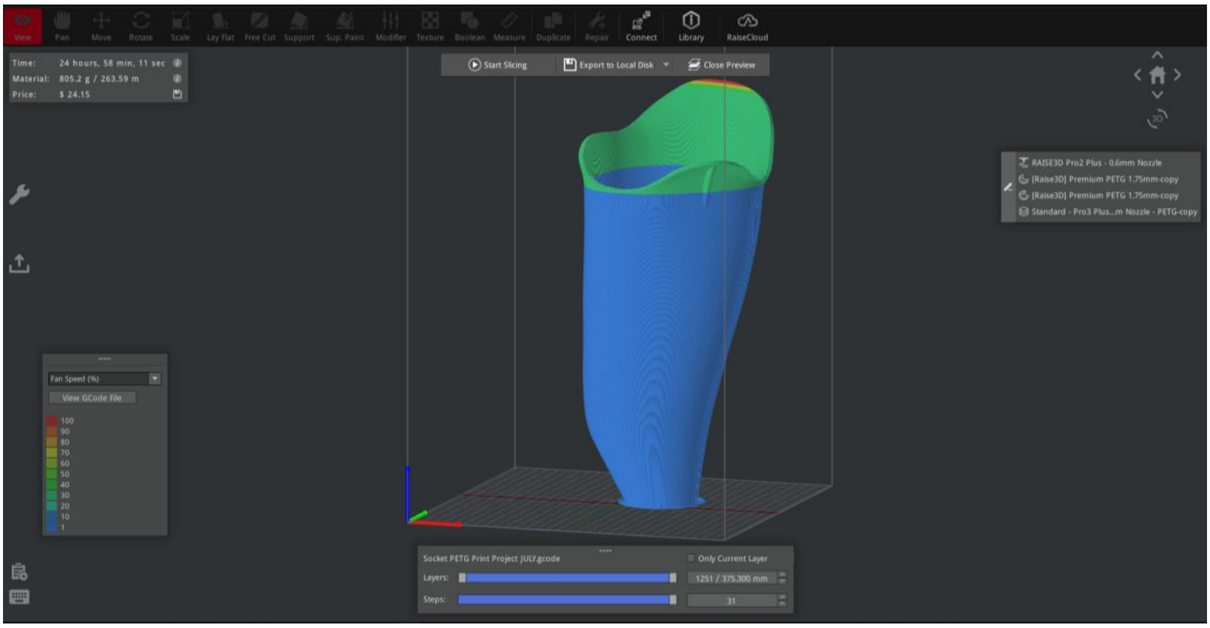

Figure D.22: Slicer fan speed settings

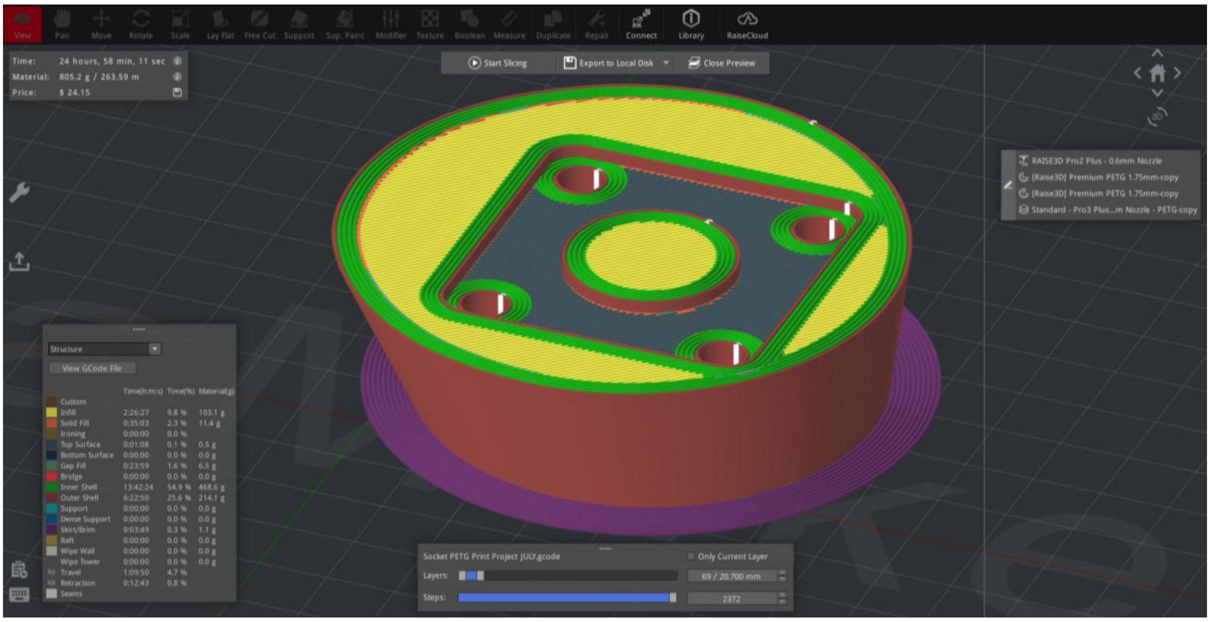

Figure D.23: Sliced view of attachment region

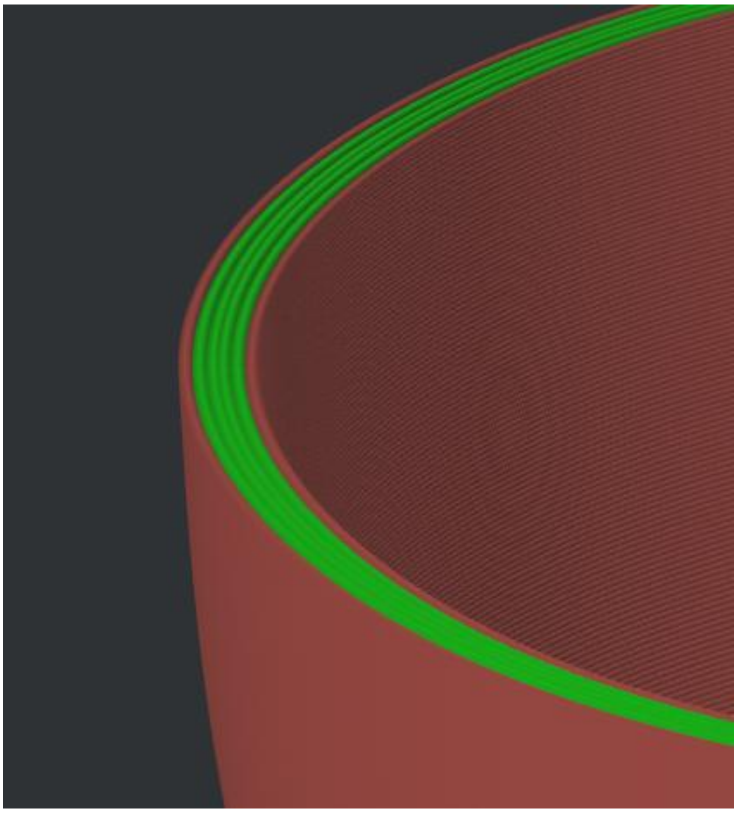

Figure D.24: Sliced view of wall printing lines